Published OnlineFirst December 26, 2017; DOI: 10.1158/0008-5472.CAN-17-1833

Tumor Biology and Immunology

Cancer Research

GADD45β Loss Ablates Innate Immunosuppression in Cancer

Daniela Verzella[1], Jason Bennett[2], Mariafausta Fischietti[1], Anil K. Thotakura[2], Camilla Recordati[3], Fabio Pasqualini[4], Daria Capece[1], Davide Vecchiotti[1], Daniel D'Andrea[2], Barbara Di Francesco[1], Marcella De Maglie[3], Federica Begalli[2], Laura Tornatore[2], Salvatore Papa[2,5], Toby Lawrence[6], Stuart J. Forbes[7], Antonio Sica[4,8], Edoardo Alesse[1], Francesca Zazzeroni[1], and Guido Franzoso[2]

Abstract

T-cell exclusion from the tumor microenvironment (TME) is a major barrier to overcoming immune escape. Here, we identify a myeloid-intrinsic mechanism governed by the NF-κB effector molecule GADD45β that restricts tumor-associated inflammation and T-cell trafficking into tumors. In various models of solid cancers refractory to immunotherapies, including hepatocellular carcinoma and ovarian adenocarcinoma, *Gadd45b* inhibition in myeloid cells restored activation of proinflammatory tumor-associated macrophages (TAM) and intratumoral immune infiltration, thereby diminishing oncogenesis. Our results provide a basis to interpret clinical evidence that elevated expression of *GADD45B* confers poor clinical outcomes in most human cancers. Furthermore, they suggest a therapeutic target in GADD45β for reprogramming TAM to overcome immunosuppression and T-cell exclusion from the TME.

Significance: These findings define a myeloid-based immune checkpoint that restricts T-cell trafficking into tumors, with potentially important therapeutic implications to generally improve the efficacy of cancer immunotherapy. *Cancer Res; 78(5); 1275–92. ©2017 AACR.*

Introduction

Virtually all tumors contain an inflammatory infiltrate of innate and adaptive immune cells (1). Despite their inherent capacity to counter neoplastic progression and eliminate nascent tumors, these cells, especially those of the innate immune system, often have the effect of promoting oncogenesis (1, 2). Accordingly, tumor-associated inflammation is now considered a hallmark of cancer (1). The ability of the immune system to influence oncogenesis is currently being exploited to treat cancer patients, with the development of many successful anticancer immunotherapies (3). Indeed, therapies blocking pivotal immunoinhibitory mechanisms, comprising immune checkpoint molecules, for example, cytotoxic T lymphocyte antigen-4 (CTLA-4) or programmed cell death protein 1 (PD-1), are revolutionizing the clinical management of certain malignancies, such as metastatic melanoma (4). However, major challenges remain, as the majority of patients rarely exhibit an objective response to these treatments, due to the absence of a preexisting intratumoral T-cell infiltrate or, in patients with T-cell–infiltrated tumors, the dominant inhibitory effects of additional tumor microenvironment (TME)–associated molecules (3, 5). Yet, the mechanisms underlying the immunoinhibitory activities of the TME are presently poorly understood.

Tumor-associated macrophages (TAM) are implicated in various TME-mediated mechanisms that enable cancers to evade immune attack (3, 6, 7). TAMs are the main leukocyte population found in most human tumors, where they play a key role in restricting local T-cell trafficking and T-cell effector functions (3, 6, 7). Indeed, a high density of TAMs, especially those exhibiting an anti-inflammatory and immunosuppressive phenotype, correlates with poor clinical outcome in most human cancers (7, 8). Accordingly, therapeutic approaches limiting myeloid cell recruitment into tumors have resulted in increased TME-based $CD8^+$ effector T-cell infiltration and diminished tumor burden in mouse models and early-phase clinical trials (3, 6, 9–13). However, the general macrophage depletion associated with these approaches raises important safety concerns. Therefore, a preferable approach would be to reprogram TAMs toward

[1]Department of Biotechnological and Applied Clinical Sciences, University of L'Aquila, L'Aquila, Italy. [2]Centre for Cell Signalling and Inflammation, Department of Medicine, Imperial College London, London, United Kingdom. [3]Mouse & Animal Pathology Laboratory, Fondazione Filarete, Milan, Italy. [4]Department of Inflammation and Immunology, Humanitas Clinical and Research Center, Rozzano, Milan, Italy. [5]Current address: Leeds Institute of Cancer and Pathology (LICAP), University of Leeds, Leeds, United Kingdom. [6]Centre d'Immunologie de Marseille-Luminy, Aix Marseille Université, Inserm, CNRS, Marseille, France. [7]Medical Research Council Centre for Regenerative Medicine, University of Edinburgh, Edinburgh, United Kingdom. [8]Department of Pharmaceutical Sciences, Università del Piemonte Orientale 'Amedeo Avogadro', Novara, Italy

Note: Supplementary data for this article are available at Cancer Research Online (http://cancerres.aacrjournals.org/).

D. Verzella, J. Bennett, M. Fischietti, and A.K. Thotakura are co-first authors of this article.

F. Zazzeroni and G. Franzoso are co-last authors of this article.

Corresponding Authors: Guido Franzoso, Imperial College London, Room 10N8, Commonwealth Building, Hammersmith Campus, Du Cane Road, London, W12 0NN, United Kingdom. Phone: 44-0-20-3313-8421; Fax: 44-0-20-83832788; E-mail: g.franzoso@imperial.ac.uk; Francesca Zazzeroni, Department of Biotechnological and Applied Clinical Sciences, University of L'Aquila, Via Vetoio 10 – Coppito II, L'Aquila 67100, Italy. Phone: 39-0862-433526; Fax: 39-0862-433523; E-mail: francesca.zazzeroni@univaq.it

doi: 10.1158/0008-5472.CAN-17-1833

Published OnlineFirst December 26, 2017; DOI: 10.1158/0008-5472.CAN-17-1833

a proinflammatory phenotype capable of redirecting T-cell trafficking into tumors and unleashing local antitumor immune responses (6, 14).

Macrophages can differentiate into a spectrum of phenotypic states in response to diverse environmental signals. At sites of infection, "classically" activated or proinflammatory macrophages (hereafter also occasionally referred to as M1-like macrophages) arise in response to IFNγ and Toll-like receptor (TLR) ligands to eliminate invading pathogens, promote inflammation, and engage the adaptive immune system. In contrast, "alternatively" activated or anti-inflammatory macrophages (hereafter also occasionally referred to as M2-like macrophages) are "educated" by IL4 and IL13 at sites of injury to terminate inflammation and enable wound healing (7, 8). Interestingly, anti-inflammatory macrophages resemble the TAMs found in most human cancers, where they support tumor progression, metastatic dissemination, and cancer immune evasion (7, 8). However, little is known about the mechanisms governing the opposing functions of macrophages in response to tissue injury, malignancy, or infection. Consequently, there are presently no therapeutic agents capable of effectively reprogramming TAMs to oppose oncogenesis.

Recent studies have identified NF-κB transcription factors as key determinants in the balance between proinflammatory and anti-inflammatory macrophage activation in response to infection or tumor-derived signals (15, 16). In fact, in addition to orchestrating protective immune and inflammatory responses, the NF-κB pathway drives oncogenesis in multiple cancer types by suppressing apoptosis of tumor cells and, concurrently, governing TME-based inflammation, thereby serving as a central hub linking cancer and inflammation (16, 17). In ovarian adenocarcinoma models, macrophage-specific inhibition of the NF-κB–activating kinase, IκBα kinase (IKK)β, was shown to reverse the anti-inflammatory TAM phenotype and enhance proinflammatory macrophage activation, thereby causing tumor regression (18). A similar conversion from an anti-inflammatory TAM activation state supportive of oncogenesis to a proinflammatory activation state that antagonizes tumor growth was reported in melanoma and fibrosarcoma models in mice bearing TAMs lacking NF-κB1/p105 (19). Notably, this IKKβ/NF-κB function in suppressing proinflammatory activation was shown to extend beyond the cancer context, reflecting the tissue-specific role that IKKβ/NF-κB plays in myeloid cells, where opposite to its conventional proinflammatory role, NF-κB drives the resolution of inflammation to enable wound healing and prevent tissue damage (20, 21).

Therefore, the IKKβ/NF-κB pathway provides an attractive route to therapeutically reverse TME-mediated immunosuppression by reprogramming TAMs toward a proinflammatory phenotype (15, 18). However, therapeutically targeting this pathway with conventional IKKβ/NF-κB inhibitors has not proven possible, due to the severe on-target toxicities associated with globally suppressing NF-κB (17). A logical alternative to pharmacologically inhibiting IKKβ/NF-κB would be therefore to target the nonredundant downstream effectors of the NF-κB anti-inflammatory function in myelomonocytic cells. However, these effectors and their modes of action remain poorly understood.

Here, we report that the NF-κB–regulated protein, GADD45β (22, 23), mediates an essential myeloid-intrinsic mechanism governing proinflammatory macrophage activation and the immunosuppressive activity of the TME that restrict $CD8^+$ T-cell trafficking into tumors. Using three distinct models of solid cancers that are largely refractory to immunotherapies, including hepatocellular carcinoma (HCC) and ovarian adenocarcinoma, we showed that *Gadd45b* deletion in myeloid cells restores proinflammatory TAM activation and intratumoral $CD8^+$ T-lymphocyte infiltration, resulting in diminished tumor growth. Because we previously showed that GADD45β additionally mediates the NF-κB antiapoptotic activity in cancer cells (24), our current findings identify GADD45β as a pivotal downstream hub integrating the NF-κB oncogenic functions linking cancer and inflammation. Our finding that elevated *GADD45B* expression correlates with poor clinical outcomes across most human cancers consolidates the general clinical significance of the GADD45β-mediated oncogenic mechanism in malignant disease. Together, these results reveal a pathogenically critical, innate immunity "checkpoint" governed by GADD45β that is amenable to therapeutic intervention to "re-educate" TAMs and ultimately overcome TME-dependent immunosuppression, with profound implications for anticancer therapy.

Materials and Methods

Human cancer datasets

The human datasets of lung cancer (LUNG), stomach adenocarcinoma (STAD), nonalcoholic liver hepatocellular carcinoma (LIHC), esophageal carcinoma (ESCA), cervical carcinoma (CESC), untreated primary glioblastoma multiforme (GBM), cholangiocarcinoma (CHOL), head and neck squamous cell carcinoma (HNSC), and kidney clear cell carcinoma (KIRC) were part of The Cancer Genome Atlas (25) program and downloaded from the UCSC Cancer Genomic Browser (26). Gene expression profiling was performed on fresh or frozen tissue biopsies using the Illumina HiSeq 2000 RNA Sequencing platform. The estimates of *GADD45B* expression levels were derived from the normalized values in the UCSC Cancer Genomic Browser. The datasets of colon adenocarcinoma (COAD; GSE39582), bladder carcinoma (BLCA; GSE13507) and ovarian cancer (OV; GSE9891) were deposited in the National Center for Biotechnology Information (NCBI) Gene Expression Omnibus (GEO) database (www.ncbi.nlm.nih.gov/geo). The COAD dataset was from the French national Cartes d'Identité des Tumeurs (CIT) program and generated using the Affymetrix Human Genome U133 Plus 2.0 Array platform (27). The BLCA dataset was from the Chungbuk National University Hospital (Cheongju, South Korea) and generated using the Illumina human-6 v2.0 expression beadchip platform (28). The OV dataset was from the Australian Ovarian Cancer Study, Royal Brisbane Hospital (Queensland, Australia), Westmead Hospital (Sydney, Australia), and Netherlands Cancer Institute (Amsterdam, Netherlands) and generated using the Affymetrix Human Genome U133 Plus 2.0 Array platform (29). The relative *GADD45B* mRNA expression levels in these datasets were derived from the normalized values present in the GEO database. The breast carcinoma dataset (BRCA) was from the tumor banks in the United Kingdom and Canada, and gene profiling data were generated using the Illumina HumanHT-12 V3 platform and deposited on Oncomine Research Premium Edition (30).

The gene profiling data from each dataset were downloaded together with the accompanying clinical information. Where possible, the series were obtained from patients at an early disease stage and datasets with a sufficient number of patients with recurrence-free survival (RFS) information. In the other cases,

Published OnlineFirst December 26, 2017; DOI: 10.1158/0008-5472.CAN-17-1833

where this was not possible, the series consisted of overall survival (OS) data and/or the entire patient dataset. Patients were stratified into two groups on the basis of the *GADD45B* mRNA expression levels. In each case, quintiles, quartiles, tertiles, and 95th percentiles were used as thresholds, and the best fits are reported in Fig. 1A–M.

Cell culture and macrophage isolation and treatment

The C57BL/6 mouse fibrosarcoma cell line, MCA-203, was kindly provided by I. Marigo and V. Bronte (Department of Oncology and Surgical Sciences, University of Padua, Padua, Italy) and cultured in high-glucose DMEM (with L-glutamine, without sodium pyruvate; Gibco) supplemented with 10% heat-inactivated FBS (Sigma-Aldrich), antibiotics (150 U/mL penicillin, 200 U/mL streptomycin), 10 mmol/L HEPES (Gibco), 2 μmol/L β-mercaptoethanol, and 2 mmol/L L-glutamine (Gibco). The C57BL/6 mouse ovarian carcinoma cell line, ID8-Luc, stably expressing firefly luciferase (Luc), was described previously (18) and cultured in high-glucose DMEM (with L-glutamine, without sodium pyruvate; Gibco) supplemented with 4% heat-inactivated FBS (Sigma-Aldrich), antibiotics (150 U/mL penicillin, 200 U/mL streptomycin), ITS+1 Liquid Media Supplement (5 μg/mL insulin, 5 μg/mL transferrin, 5 ng/mL sodium selenite; Sigma-Aldrich), and 2 mmol/L L-glutamine (Gibco). Cells were cultured in a humidified incubator in 5% CO_2 at 37°C. All cell lines were routinely tested using a Mycoplasma Detection Kit (ATCC). Before injection *in vivo*, cell lines were also routinely screened for other infectious agents using the Mouse Essential CLEAR Panel (Charles River Laboratories). The cell line authentication for the MCA-203 and ID8-Luc murine cell lines has not been possible because these cell lines are not commercially available. Cells were used for the experiments between 5 and 7 days upon thawing.

Bone marrow–derived macrophages (BMDM) were prepared from 6- to 10-week old *Gadd45b*$^{-/-}$ and *Gadd45b*$^{+/+}$ C57BL/6J mice as described previously (21). BMDMs were treated with LPS (*E. coli* serotype O55:B5, 100 ng/mL; Sigma-Aldrich) and mouse recombinant IFNγ (20 ng/mL; Sigma-Aldrich) or with mouse recombinant IL4 (20 ng/mL; Peprotech) and mouse recombinant IL13 (20 ng/mL; Peprotech). The p38 inhibitors used were Vx745 (20 μmol/L; Selleckchem), Skepinone-L (10 μmol/L; Selleckchem), and SB203580 (20 μmol/L; Cell Signaling Technology).

For TAM isolation, intraperitoneal cells were harvested from ID8-Luc tumor-bearing mice by peritoneal lavage with 1× PBS and passed through a 70-μm cell strainer (BD Biosciences), following red blood cell removal with RBC lysis buffer (Sigma-Aldrich). TAMs were separated using MACS MicroBead Technology (Miltenyi Biotec) by negative selection with anti–Ly-6G MicroBead Kit, mouse, followed by positive selection with CD11b MicroBeads, human and mouse (Miltenyi Biotec), according to the manufacturer's instructions.

Further information on the procedures for BMDM isolation can be found in the Supplementary Information.

BMDM/tumor cell coculture

Gadd45b$^{-/-}$ and *Gadd45b*$^{+/+}$ BMDMs were prepared as above and cocultured with ID8-Luc or MCA-203 tumor cells, without direct cell-to-cell contact, according to established protocols (18, 31). Further information on the procedures for BMDM/tumor cell coculture can be found in the Supplementary Information.

Mice

C57BL/6Jx129/SvJ *Gadd45b*$^{-/-}$ mice were described previously (32). *Gadd45b*$^{+/+}$ littermates were cohoused and used as controls. C57BL/6J *Gadd45b*$^{-/-}$ and *Gadd45b*$^{+/+}$ mice were obtained by backcrossing the corresponding C57BL/6Jx129/SvJ lines onto C57BL/6J to at least the N14 backcross generation. C57BL/6J CD45.1/Ly5.1^{+} mice (B6.SJL-*Ptprc*^{a} *Pepc*^{b}/BoyJ) and C57BL/6J LysM-cre transgenic mice were purchased from The Jackson Laboratory. C57BL/6J *Gadd45b*$^{-/-}$ and *Gadd45b*$^{+/+}$ mice, expressing either CD45.2/Ly5.2^{+} or CD45.1/Ly5.1^{+}, were cohoused and bred as separate colonies.

Conditional *Gadd45b* knockout mice, carrying loxP-flanked *Gadd45b* alleles (*Gadd45b*^{F}), were generated at Taconic Biosciences using conventional gene targeting technology in embryonic stem (ES) cells. Homozygous *Gadd45b*$^{F/F}$ mice were obtained by the interbreeding of *Gadd45b*$^{F/+}$ mice. *Gadd45b*$^{\Delta M/\Delta M}$ mice, specifically lacking *Gadd45b* in the myeloid lineage, were generated by crossing *Gadd45b*$^{F/F}$ mice with C57BL/6J LysM-cre mice (The Jackson Laboratory), expressing a Cre recombinase transgene under the control of the myeloid-specific *LysM* promoter (33). Cohoused *Gadd45b*$^{F/F}$ littermates were used as controls for the experiments.

Mice were housed in ventilated cages in a pathogen-free mouse facility of the Central Biomedical Services at Imperial College London (London, United KIngdom) and used in accordance with established institutional guidelines, under the authority of UK Home Office project license, P75F16A53 [see Guidelines on the Operation of Animals (Scientific Procedures) Act of 1986]. Separate mouse colonies were maintained in filtered top cages on autoclaved food, water, and bedding in the Conventional Mouse Facility at the University of L'Aquila (L'Aquila, Italy), and experimental procedures were performed in accordance with national and international laws and regulations (see European Economic Community Council Directive 86/609, OJ L 358, 1, December 12, 1987; Italian Legislative Decree 116/92, Gazzetta Ufficiale della Republica Italiana no.40, February 18, 1992; National Institutes of Health Publication no.85-23, 1985), under the approval of the University of L'Aquila Internal Committee and the Italian Ministry of Health.

Further information on the procedures used for the generation of *Gadd45b*$^{F/F}$ mice can be found in the Supplementary Information.

Bone marrow chimeras

Congenic CD45.1/Ly5.1^{+}*Gadd45b*$^{-/-}$ and *Gadd45b*$^{+/+}$ mice were generated by crossing the corresponding C57BL/6J lines (CD45.2/Ly5.2^{+}) with C57BL/6J B6.SJL-*Ptprc*^{a} *Pepc*^{b}/BoyJ mice (The Jackson Laboratory), carrying homozygous *Ptprc*^{a} (*CD45.1/Ly5.1*) alleles and used as donors in bone marrow adoptive transfer experiments to distinguish between hematopoietic-derived cells of recipient (CD45.2/Ly5.2^{+}) and donor (CD45.1/Ly5.1^{+}) origin. For these experiments, bone marrow cells were harvested from femurs and tibiae of 6- to 10-week old CD45.1/Ly5.1^{+}*Gadd45b*$^{-/-}$ or *Gadd45b*$^{+/+}$ males under aseptic conditions. Red blood cells were lysed using RBC lysis buffer (Sigma-Aldrich), washed in serum-free medium, counted, and resuspended in 1× PBS. 4 (Protocol A) or 16 (Protocol B)-week-old C57BL/6J *Gadd45b*$^{-/-}$ and *Gadd45b*$^{+/+}$ male recipients, carrying *Ptprc*^{b} (*CD45.2/Ly5.2*) alleles, were lethally irradiated with a single dose of 9.5 Gy and, 24 hours later, intravenously injected via the tail vein with 5×10^{6} bone marrow donor cells, to generate all four

Published OnlineFirst December 26, 2017; DOI: 10.1158/0008-5472.CAN-17-1833

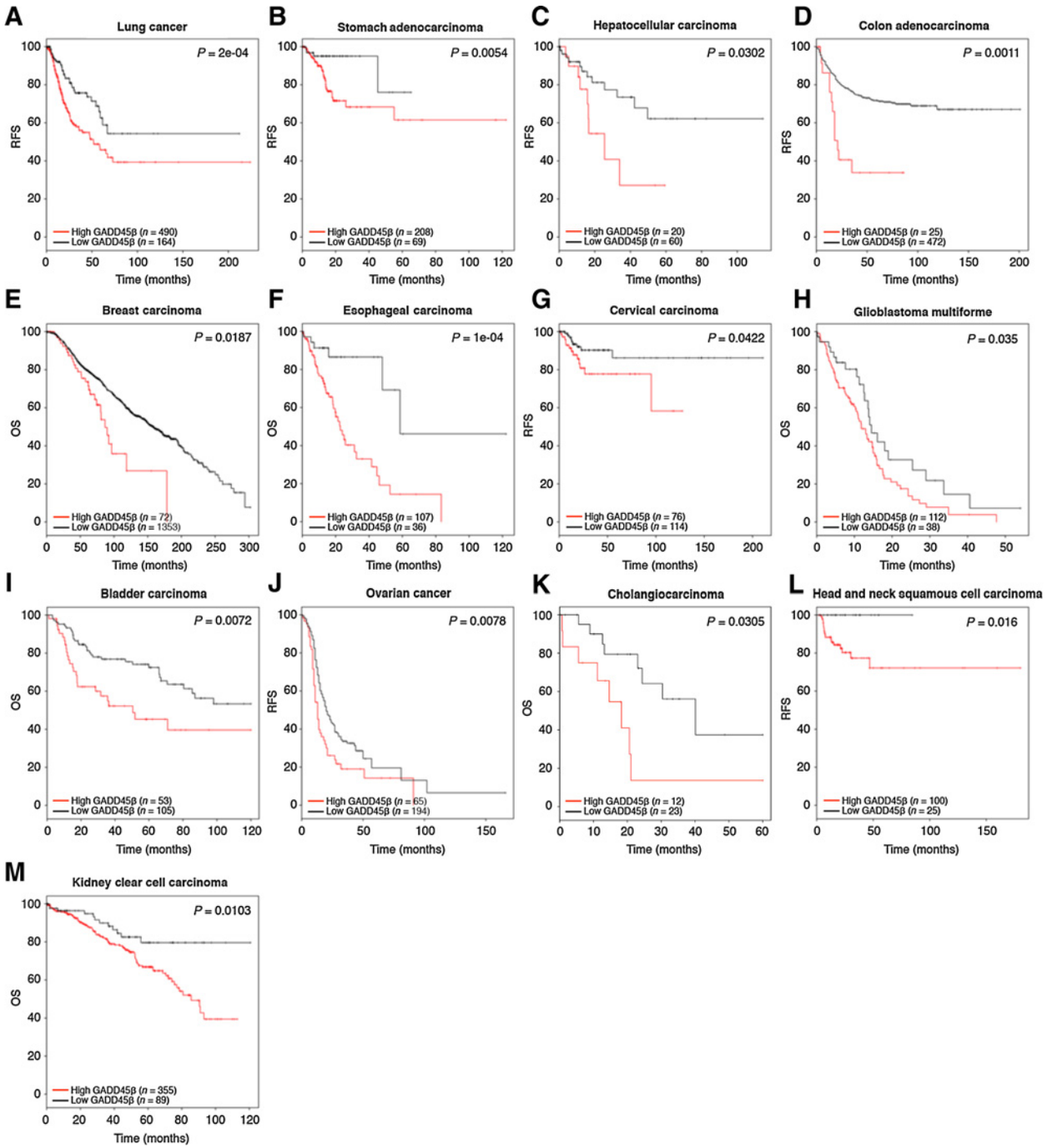

Figure 1.

The widespread correlation between elevated *GADD45B* expression and poor clinical outcome across human cancer types. **A–M,** RFS and OS in patients with the indicated malignant pathologies, representing 13 of the top 15 solid cancers for mortality worldwide and deposited in the following publicly available datasets: The Cancer Genome Atlas program (**A**, **B**, **C**, **F**, **G**, **H**, **K**, **L**, and **M**); the French National Cartes d'Identité des Tumeurs program (**D**); the Tumour Banks in the United Kingdom and Canada (**E**); the Chungbuk National University Hospital (**I**); and the Australian Ovarian Cancer Study, Royal Brisbane Hospital, Westmead Hospital and Netherlands Cancer Institute (**J**). Patients in each series were stratified at diagnosis in two groups on the basis of the *GADD45B* mRNA expression in the tumor tissues, as shown. *P* values are indicated.

possible chimerism combinations. Bone marrow reconstitution with CD45.1/Ly5.1^{+} donor cells was verified after adoptive transfer by FACS analysis of blood leukocytes.

DEN treatment and HCC induction

For the initiation-only model of HCC, 15- to 17-day old *Gadd45b*$^{-/-}$ and *Gadd45b*$^{+/+}$ males on a C57Bl/6Jx129/SvJ or

Published OnlineFirst December 26, 2017; DOI: 10.1158/0008-5472.CAN-17-1833

C57Bl/6J background, as indicated, were injected intraperitoneally with a single dose of diethylnitrosamine (DEN; 5 and 20 mg/kg, respectively; Sigma-Aldrich). At the indicated endpoints, mice were sacrificed and their livers removed, photographed, and separated into individual lobes. Externally visible tumors (≥0.5 mm) were measured using a caliper and counted. Tumor areas were calculated using the formula: π(diameter 1 + diameter 2)^2/4 (34). For histologic evaluations, liver tissue was fixed in 10% neutral-buffered formalin solution and paraffin embedded. The remaining liver tissue was microdissected into tumor and nontumor tissue and stored at −80°C for molecular evaluation.

For HCC induction in the tumor initiation–promotion model, mice were treated according to two distinct experimental setups, designated as Protocol A and Protocol B. As part of Protocol A, 4-week-old C57BL/6J males (CD45.2/Ly5.2$^+$) were adoptively transferred with bone marrow from CD45.1/Ly5.1$^+$ males, and, 4 weeks later, intravenously treated twice with of 200 μL of clodronate liposomes to deplete endogenous Kupffer cells. Clodronate liposomes, containing approximately 5 mg/mL of clodronate, were prepared as described previously and were provided by N. Van Rooijen (ClodronateLiposomes.org; ref. 35). Ten weeks after clodronate liposome administration, bone marrow chimeras were intraperitoneally injected with a single dose of DEN (100 mg/kg; Sigma-Aldrich) and, 4 weeks later, placed on treatment with 0.07% of the tumor promoter, phenobarbital (Sigma-Aldrich), in the drinking water until the experimental endpoint, according to an established tumor initiation–promotion protocol (33). As part of Protocol B, 4-week-old C57BL/6J males (CD45.2/Ly5.2$^+$) were intraperitoneally injected with 75 mg/kg of DEN (Sigma-Aldrich) and, 4 weeks later, placed on treatment with 0.07% phenobarbital (Sigma-Aldrich) in the drinking water, as above, to induce HCC initiation and early promotion. After 8 weeks, mice were adoptively transferred with bone marrow from congenic CD45.1/Ly5.1$^+$ males and, 4 weeks later, treated with 200 μL of clodronate liposomes, as above, to deplete Kupffer cells. At the indicated endpoints, mice were sacrificed, and their livers removed, photographed, and separated into individual lobes. Externally visible tumors (≥0.5 mm) were counted. For histologic evaluations, liver tissue was fixed and paraffin-embedded or embedded in Tissue-Tek OCT compound (Sakura Finetek) for frozen block preparation. Bone marrow–cell reconstitution and liver repopulation with donor-derived CD45.1/Ly5.1$^+$ Kupffer cells were confirmed in each group of bone marrow chimaeras by FACS analysis of spleen and bone marrow cells and immunofluorescence staining of frozen liver sections, respectively.

To validate the procedure for Kupffer cell depletion, a separate group of C57BL/6J mice was intravenously injected with a single dose of 200 μL of clodronate or PBS liposomes. At the indicated time points, mice were sacrificed, and their livers and spleens were removed, fixed and paraffin-embedded for immunohistologic evaluation of macrophage depletion.

Tumor allografts

For fibrosarcoma allografts, 6- to 8-week-old C57BL/6J *Gadd45b*$^{-/-}$ and *Gadd45b*$^{+/+}$ males were subcutaneously injected in the right flank with 1.0 × 10^5 MCA-203 cells in 100 μL of sterile 1× PBS, using a 1-mL Leur-Lok Tip syringe (BD Biosciences) with a 25-guage needle. MCA-203 cells were harvested from exponentially growing cultures, washed once with serum-free medium, and resuspended in 1× PBS immediately before injection. Once tumors became palpable, tumor growth was monitored every other day using a vernier caliper. Tumor volumes were calculated using the formula: volume = $A \times B^2/2$ (where A is the larger diameter, and B is the smaller diameter of the tumor; ref. 24). Nineteen days after tumor cell injection, mice were sacrificed, and tumors were removed and embedded in Tissue-Tek OCT compound (Sakura Finetek) for frozen block preparation. To investigate the macrophage-specific role of GADD45β in sarcomagenesis, 6- to 8-week-old *Gadd45b*$^{F/F}$ and *Gadd45b*$^{\Delta/\Delta}$ males were injected with 1.0 × 10^5 exponentially growing MCA-203 cells in 200 μL of sterile 1× PBS containing Matrigel (1:1; Corning). Tumor growth was monitored using a vernier caliper, and tumor volumes were calculated as above. At the indicated endpoint, mice were sacrificed, and tumors were photographed.

For the *in vivo* depletion of CD8$^+$ T cells, 8- to 12-week-old C57BL/6J *Gadd45b*$^{-/-}$ and *Gadd45b*$^{+/+}$ female mice were treated intraperitoneally with 250 μg of anti-CD8b antibody (Lyt 3.2; clone 53-5.8; Bio X Cell) or rat IgG isotype-matched control antibody (clone HRPN; Bio X Cell) at day −1 and day 0 before the injection of 1.0 × 10^5 exponentially growing MCA-203 cells prepared as described above, and then twice a week with the same dose of antibody until the experimental endpoint. Tumor growth was monitored as described above. The efficiency of the antibody-mediated CD8$^+$ T-cell depletion was determined by FACS analysis of spleen cells using anti–CD8b-APC (130-106-315), anti–CD4-APC (130-109-415), and anti–CD3-FITC (130-108-836) antibodies (Miltenyi Biotec).

For ovarian carcinoma allografts, 11- to 12-week-old C57BL/6J *Gadd45b*$^{-/-}$ and *Gadd45b*$^{+/+}$ females were intraperitoneally injected with exponentially growing 1.0 × 10^6 ID8-Luc cells in 300 μL of sterile saline solution, using a 1-mL Leur-Lok Tip syringe (BD Biosciences) with a 25-guage needle. Tumor growth was monitored weekly starting 6 weeks after tumor cell injection by bioluminescence imaging.

The analyses of the macrophage-specific role of GADD45β in ovarian oncogenesis were performed essentially as described previously (18). Briefly, 8-week-old C57BL/6J *Gadd45b*$^{+/+}$ females (Harlan Laboratories) were intraperitoneally injected with 2 × 10^6 exponentially growing ID8-Luc cells in 300 μL of sterile saline solution, and tumors were allowed to grow, as above. After 5 weeks, mice were randomized into two groups and intraperitoneally injected with 10 × 10^6 BMDMs from C57BL/6J *Gadd45b*$^{-/-}$ or *Gadd45b*$^{+/+}$ mice in 300 μL of sterile saline solution. ID8-Luc tumor growth was monitored weekly by bioluminescence imaging. Further information on the procedures used for bioimaging can be found in the Supplementary Information.

Histopathologic analyses, IHC, immunofluorescence, and TUNEL assays

Detailed information on the procedures used for histopathologic analyses, IHC, immunofluorescence, and TUNEL assays can be found in the Supplementary Information.

qRT-PCR analysis, Western blots, and FACS analysis

Detailed information on the procedures used for RNA extraction, qRT-PCR reactions, Western blotting, and FACS analysis can be found in the Supplementary Information.

Published OnlineFirst December 26, 2017; DOI: 10.1158/0008-5472.CAN-17-1833

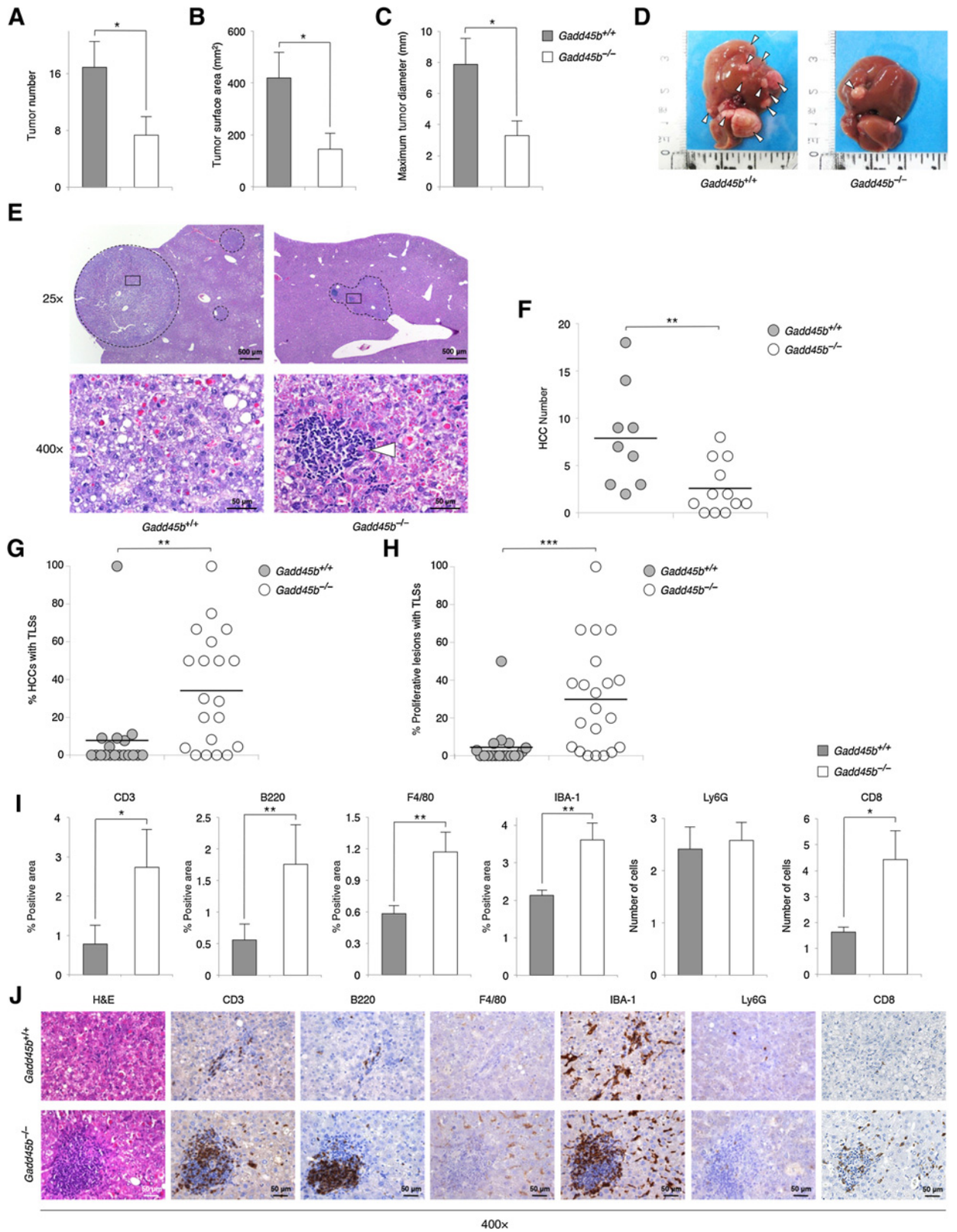

Published OnlineFirst December 26, 2017; DOI: 10.1158/0008-5472.CAN-17-1833

Statistical analysis

Data were analyzed using GraphPad Prism version 7.0 (GraphPad Software) or R (www.R-project.org). Statistical analyses of the results were performed using either two-tailed *t* tests or two-tailed Mann–Whitney *U* test, depending on the distribution of the data. Assumptions concerning the data (e.g., normal distribution and similar variation between experimental groups) were examined for appropriateness before statistical tests were conducted. *P* values <0.05 were considered statistically significant. For ovarian carcinoma allografts, outliers were detected and removed according to the default options of the software used.

Survival analyses were performed in R, using package survival. Differences between the survival distributions within each dataset were assessed for statistical significance using Kaplan–Meier curves and the log-rank test, with $P < 0.05$ taken as the level of significance.

For the sample size of the animals used in this study, it was fixed in a prospective manner; no statistical method was used to predetermine sample size. Mice with the indicated genotypes were included in the study without any randomization. Histologic analyses were performed in a single-blinded fashion. No blinding was used for the remaining analyses.

Results

GADD45B expression denotes aggressive malignant disease across most human cancers

We recently identified the product of the NF-κB–regulated gene, *GADD45B*, as an essential survival factor and novel therapeutic target in multiple myeloma (24). We therefore investigated whether *GADD45B* was involved in any types of malignancy beyond multiple myeloma. Strikingly, in publicly available patient datasets, elevated *GADD45B* expression correlated with rapid disease progression in 13 of the top 15 solid cancers for mortality worldwide (36). When patients with prevalent disease subtypes were stratified at diagnosis on the basis of *GADD45B* expression in the tumor tissues, the patient cohorts expressing high *GADD45B* levels exhibited significantly shorter RFS and/or OS than the corresponding cohorts expressing low *GADD45B* mRNA levels (Fig. 1A–M). Collectively, these results identify GADD45β as a hallmark of aggressive pathology across the most prevalent human cancer types and postulate its general clinical significance in malignant disease.

Gadd45b loss reduces chemically induced hepatocellular carcinogenesis

The role of IKKβ/NF-κB in hepatocellular carcinogenesis is controversial (16, 17). Indeed, in the widely used DEN experimental model of HCC, hepatocyte-specific *Ikkb* ablation was previously shown to promote, rather than inhibit, oncogenesis (33). Therefore, to clarify the basis for the observed correlation between expression of the IKKβ/NF-κB–regulated effector, *GADD45B*, and aggressive disease pathology in HCC datasets (Fig. 1C), we sought to investigate whether GADD45β was involved in this process. Fifteen-day-old $Gadd45b^{-/-}$ and $Gadd45b^{+/+}$ C57BL76J males were treated with a single intraperitoneal injection of the carcinogen, DEN, according to an established protocol for HCC induction (33). As expected, all $Gadd45b^{+/+}$ mice given DEN developed typical HCCs within 9 months (Fig. 2A–E). Interestingly, *Gadd45b* deletion significantly reduced the number of HCCs (Fig. 2A and D). Tumor surface area and maximum tumor diameter were also markedly reduced in $Gadd45b^{-/-}$ mice relative to controls (Fig. 2B and C).

Histologic analysis confirmed the more than 3-fold lower number of HCCs in $Gadd45b^{-/-}$ than $Gadd45b^{+/+}$ livers (Fig. 2F). As typically seen in C57BL76J mice, DEN-induced tumors predominantly consisted of adenomas, with only few sporadic carcinomas, hereafter collectively referred to as HCCs. Similar results were obtained using 129/SvJxC57BL/6J mice (Supplementary Fig. S1A–S1F). Notably, $Gadd45b^{-/-}$ and $Gadd45b^{+/+}$ HCCs displayed no difference with respect to tumor grade, mitotic index, or necrosis grade, and similar percentages of proliferating and apoptotic cells (Supplementary Fig. S1G–S1J). Likewise, the analysis of cell-cycle regulators and oncogenic factors showed no difference between $Gadd45b^{-/-}$ and $Gadd45b^{+/+}$ livers when comparing corresponding tumor or nontumor tissues (Supplementary Fig. S1K). Hence, opposite to hepatocyte-specific *Ikkb* loss (33), *Gadd45b* ablation inhibits DEN-induced hepatocellular carcinogenesis, while having no effect on tumor cell proliferation or apoptosis.

Gadd45b loss augments tumor-associated macrophage and T-cell infiltration and TLS formation

Despite the otherwise similar histologic and molecular characteristics (Fig. 2E; Supplementary Figs. S1E and S1G–S1K), $Gadd45b^{-/-}$ HCCs contained considerably more and larger immunoinflammatory infiltrates than $Gadd45b^{+/+}$ tumors (Fig. 2G; see also Fig. 2E and H; Supplementary Fig. S1E). Strikingly, in $Gadd45b^{-/-}$, but not $Gadd45b^{+/+}$ HCCs, intratumoral infiltrates were also often organized into follicle-like aggregates, reminiscent of tertiary lymphoid structures (TLS; Fig. 2G–J; see also Fig. 2E; Supplementary Figs. S1E and S2A and S2B), denoting sites of thriving adaptive immune reactions and favorable clinical outcome in multiple human cancers (37). Consistently, whereas only 33% of $Gadd45b^{+/+}$ mice contained at least one HCC featuring TLS-like aggregates (hereafter referred to

Figure 2.

Reduced DEN-induced HCC development with increased intratumoral immunoinflammatory infiltrates and TLS formation in $Gadd45b^{-/-}$ mice. **A–C,** Number of tumors (≥0.5 mm; **A**), tumor surface area (**B**), and maximum tumor diameter (**C**) in livers of $Gadd45b^{+/+}$ ($n = 9$) and $Gadd45b^{-/-}$ ($n = 12$) C57BL/6J males 9 months after DEN injection (20 mg/kg). Values, means ± SEM. **D,** Gross liver morphology in representative mice from **A–C**. Arrowheads, tumors. **E,** Images of hematoxylin and eosin (H&E) staining showing the liver histology in representative mice from **A–C**. Hatched lines (top), tumor areas. Solid lines (top), areas magnified in the bottom. Arrowhead (bottom, right), a typical immunoinflammatory aggregate. Scales and magnifications are shown. **F,** Number of histologically confirmed HCCs per examined liver sections from individual mice in **A–C**. Each symbol represents an individual mouse. Horizontal lines, means. **G** and **H,** Percentages of HCCs (**G**) and combined HCCs and preneoplastic foci (**H**) containing TLSs in $Gadd45b^{+/+}$ ($n = 19$) and $Gadd45b^{-/-}$ ($n = 26$) 129/SvJxC57BL/6J males 11 months after DEN injection (5 mg/kg). Each symbol represents an individual mouse. Horizontal lines, means. **I,** IHC analysis showing the percentage of positive area or number of positive cells per field at ×400, as stated, of the indicated immune cell populations in HCCs from **G**. Values, means ± SEM (IBA-1: $Gadd45b^{+/+}$, $n = 47$; $Gadd45b^{-/-}$, $n = 34$. CD8: $Gadd45b^{+/+}$, $n = 37$; $Gadd45b^{-/-}$, $n = 33$. All other markers: $Gadd45b^{+/+}$, $24 \leq n \leq 26$; $Gadd45b^{-/-}$, $n = 26$ or $n = 27$). **J,** Images of hematoxylin and eosin and IHC staining of representative tumor sections from **I**. Scales and magnifications are shown. **A–C** and **F–I,** *, $P < 0.05$; **, $P < 0.01$; ***, $P < 0.001$. See also Supplementary Figs. S1 and S2.

Published OnlineFirst December 26, 2017; DOI: 10.1158/0008-5472.CAN-17-1833

as TLSs), well-organized TLSs were often found in multiple HCCs in 80% of *Gadd45b*$^{-/-}$ mice (Supplementary Fig. S2C; see also Supplementary Fig. S2D).

In both *Gadd45b*$^{-/-}$ and *Gadd45b*$^{+/+}$ HCCs, intratumoral leukocyte infiltrates predominantly consisted of lymphocytes and macrophages, with only few sparse granulocytes (Fig. 2I and J). However, *Gadd45b*$^{-/-}$ HCCs contained considerably more F4/80^{+} and IBA-1^{+} macrophages and B and T lymphocytes than *Gadd45b*$^{+/+}$ HCCs (Fig. 2I and J; see also Fig. 3A and B). Crucially, *Gadd45b* loss also increased the intratumoral infiltration by CD8^{+} T cells, a hallmark of effective antitumor immune responses (Fig. 2I and J). Interestingly, whereas the increased numbers of IBA-1^{+} macrophages and lymphocytes observed in *Gadd45b*$^{-/-}$ HCCs were mostly due to the greater frequency and larger size of TLSs, the increased intratumoral F4/80^{+} macrophage numbers were mainly attributable to the higher density of these cells outside TLSs. Plausibly, this distinct effect of *Gadd45b* loss on the F4/80^{+} macrophage distribution within the TME reflects the central role of these cells in sensing "danger" signals and antigens arising from tumor cells and processing them into cues to elicit reciprocal adaptive immune reactions (38). Irrespective of the mechanism(s), our data demonstrate that *Gadd45b* loss profoundly affects tumor-associated inflammation and macrophage and lymphocyte infiltration within DEN-induced HCCs.

Because resident liver macrophages, so-called Kupffer cells, play a central role in DEN-induced carcinogenesis through a mechanism that depends on IKK/NF-κB (17, 33), we further investigated the effect of GADD45β on TAMs. In keeping with their heightened state of inflammation, *Gadd45b*$^{-/-}$ HCCs contained a significantly higher number of myeloid-like cells expressing inflammatory markers, such as inducible nitric oxide synthase (iNOS) and cyclo-oxygenase-2 (COX-2), than *Gadd45b*$^{+/+}$ HCCs (Fig. 3A and B; Supplementary Fig. S2E; ref. 14). They also contained markedly more IBA-1^{+} macrophages within well-organized TLSs expressing MHC-II, a key antigen-presenting molecule and prototypical proinflammatory activation marker (Fig. 3C and D; see also Fig. 3A and B; Supplementary Fig. S2E; ref. 7), thus phenocopying the effects of myeloid-associated IKKβ/NF-κB inhibition on TAMs (18, 19). Underscoring the significance of these findings, *Gadd45b*$^{-/-}$ HCCs additionally displayed considerably more TLS-associated cells expressing the immunoinhibitory enzyme, indoleamine-2,3-dioxygenase (IDO; Figs. 3E and F), suggesting that the upregulation of immune checkpoint molecules, such as IDO (3, 4), could conceal the full immunostimulatory potential of *Gadd45b* loss. In contrast, *Gadd45b* deletion had no effect on alternative TAM activation, which is more typical of established neoplasias (Figs. 3A and B; see also Supplementary Fig. S2E; refs. 7, 8). Hence, *Gadd45b* loss enhances proinflammatory TAM activation within HCCs. Collectively, these findings indicate that GADD45β plays an essential role in curbing proinflammatory TAM activation, intratumoral lymphocyte infiltration and TLS formation within established neoplasias.

Gadd45b loss augments DEN-induced hepatocyte toxicity, but not hepatocyte proliferation

Although in established tumors macrophage-driven inflammation has the potential to elicit antitumor immune responses, it was shown that when it ensues in response to acute DEN-induced liver damage, this inflammation triggers compensatory hepatocyte proliferation, thereby facilitating HCC initiation (33). We therefore examined the effect of *Gadd45b* loss on the acute liver response to DEN administration. As expected, in *Gadd45b*$^{+/+}$ mice, DEN injection induced hepatocyte apoptosis at 48 hours (Supplementary Fig. S3A and S3B). The number of apoptotic hepatocytes was modestly increased, in *Gadd45b*$^{-/-}$ mice after DEN administration, but not at baseline, compared with controls (Supplementary Fig. S3A and S3B). Circulating liver enzymes, indicative of hepatocyte damage, were also higher in DEN-treated *Gadd45b*$^{-/-}$ than *Gadd45b*$^{+/+}$ mice (Supplementary Fig. S3C), even though the livers of these mice displayed similarly low numbers of dead cells (Supplementary Fig. S3D and S3E).

Because DEN-induced hepatocyte toxicity involves JNK activation (33, 39), and GADD45β has the capacity to suppress JNK signaling in the liver (32), we investigated the effects of *Gadd45b* loss on MAPK activation by DEN. As shown in Supplementary Fig. S3F, DEN induced strong JNK activation in *Gadd45b*$^{+/+}$ livers, but this activation was unaffected by *Gadd45b* loss. *Gadd45b* deficiency also had no effect on DEN-induced ERK, p38 or STAT3 signaling, nor did it have any effect on hepatocyte proliferation, either at baseline or following DEN injection (Supplementary Fig. S3G and S3H). Hence, *Gadd45b* loss mildly augments DEN-induced liver damage, but does not affect hepatocyte proliferation and is, therefore, unlikely to impact HCC development by affecting the acute liver response to DEN.

Hematopoietic cell–specific *Gadd45b* loss reduces DEN-induced carcinogenesis

Given the association between diminished HCC burden and increased intratumoral immunoinflammatory infiltration observed in *Gadd45b*$^{-/-}$ mice, we hypothesized that GADD45β promotes hepatocellular carcinogenesis by operating within immune and inflammatory cells. To distinguish between the oncogenic roles of GADD45β in the TME and the hepatic parenchyma, we generated bone marrow chimeras harboring all possible combinations of tissue-specific *Gadd45b* deficiency in the parenchymal tissue and bone marrow–derived cells (Fig. 4A). Given the importance of Kupffer cells in driving DEN-induced carcinogenesis (17, 33), chimeric mice were then treated with clodronate liposomes to deplete endogenous Kupffer cells and thereby permit liver repopulation with donor-derived Kupffer cells, following which, mice were administered DEN, along with the tumor promoter, phenobarbital (Protocol A; Fig. 4A), according to an established tumor initiation–promotion protocol (33).

Successful bone marrow–cell reconstitution and host Kupffer cell liver repopulation with donor-derived Kupffer cells were confirmed by FACS and immunofluorescence analyses, respectively (Supplementary Fig. S4A-S4B; see also Supplementary Fig. S4C). As expected, DEN-treated chimeras bearing isogenic *Gadd45b*$^{+/+}$ or *Gadd45b*$^{-/-}$ tissues (WT_{BM}:WT_{Host} and KO_{BM}:KO_{Host}, respectively) developed similar numbers of HCCs as their nontransplanted counterparts (Figs. 4B and C; see also Fig. 2A; Supplementary Fig. S1A). Notably, however, the ratio between HCC numbers in these mice was more than 5-folds (Fig. 4B; compare WT_{BM}:WT_{Host} with KO_{BM}:KO_{Host}) relative to the approximately 2-fold ratio observed in mice treated according to the tumor initiation–only protocol (Fig. 2A; Supplementary Fig. S1A), suggesting that *Gadd45b* loss has a greater impact on HCC progression than on tumor initiation (discussed below).

Strikingly, selective *Gadd45b* ablation in bone marrow–derived cells reduced the numbers of HCCs to similar levels as in isogenic *Gadd45b*$^{-/-}$ mice (Fig. 4B; compare KO_{BM}:WT_{Host} with WT_{BM}:

Published OnlineFirst December 26, 2017; DOI: 10.1158/0008-5472.CAN-17-1833

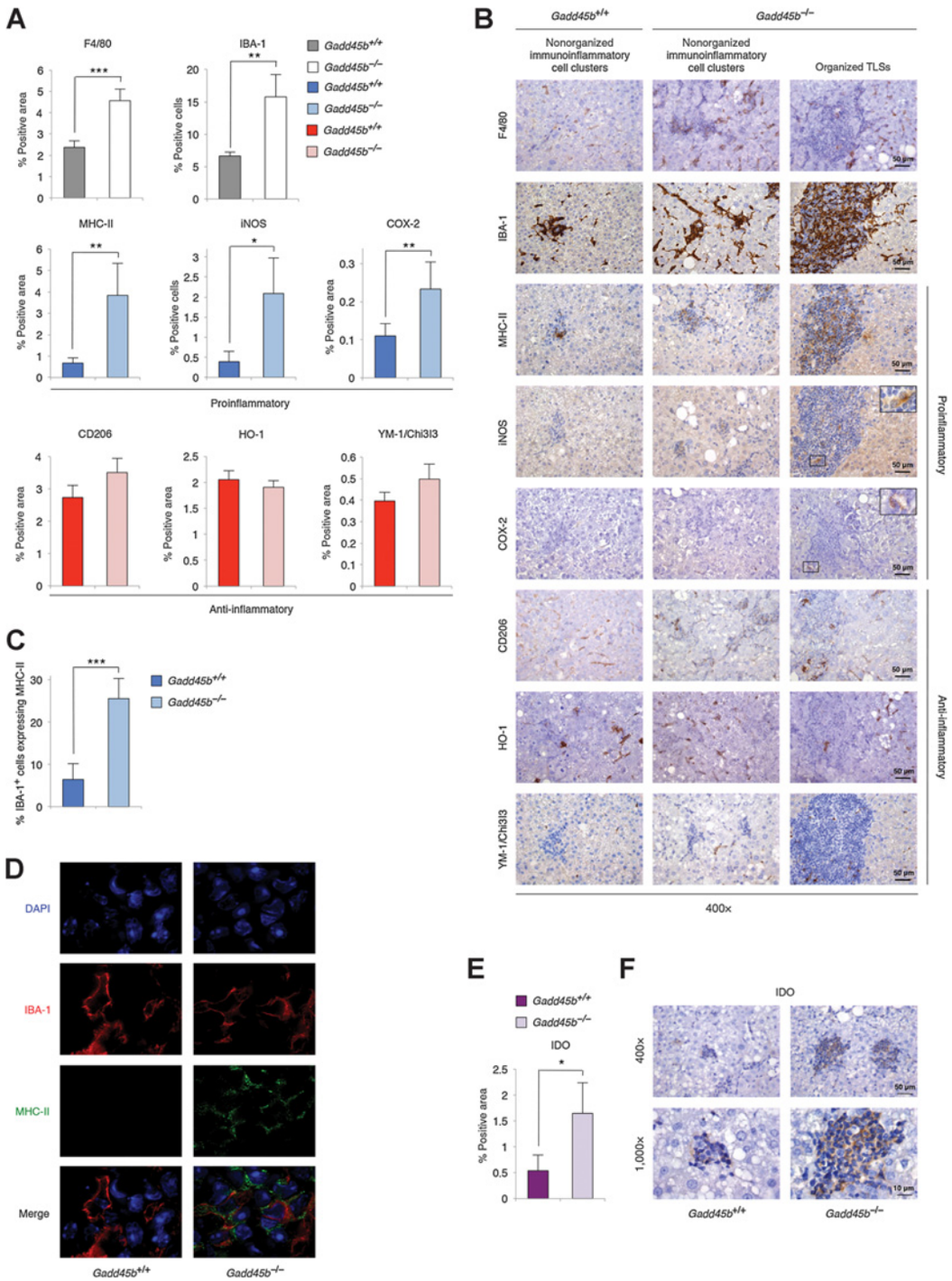

Figure 3.

Gadd45b loss increases macrophage infiltration and proinflammatory TAM activation within HCCs. **A,** IHC analysis showing the percentage of positive area or number of positive cells per field at ×400, as stated, for the indicated macrophage (F4/80, IBA-1) and proinflammatory and anti-inflammatory activation markers in HCCs from Fig. 2A–C. **B,** Images of IHC staining of representative tumor sections from **A**. Images of *Gadd45b*$^{-/-}$ HCCs are shown for nonorganized immunoinflammatory cell clusters (middle) and well-organized TLSs (right). Insets denote magnified areas at the top right corners. **C,** Immunofluorescence analysis showing the percentages of IBA-1^{+} macrophages expressing MHC-II per field at ×400 in HCCs from Fig. 2A–C. **D,** Images of immunofluorescence staining of representative tumor sections from **C**. Red, anti–IBA-1; green, anti–MHC-II; blue, DAPI. **E,** IHC analysis showing the percentage of IDO-positive area per field at ×400 in *Gadd45b*$^{+/+}$ and *Gadd45b*$^{-/-}$ HCCs from **A**. **F,** Images of IHC staining of representative tumor sections from **E**. **A**, **C**, and **E,** Values denote means ± SEM (*Gadd45b*$^{+/+}$, $14 \leq n \leq 30$; *Gadd45b*$^{-/-}$, $12 \leq n \leq 15$). *, $P < 0.05$; **, $P < 0.01$; ***, $P < 0.001$. **B**, **D**, and **F,** Scales and magnifications are shown. See also Supplementary Figs. S2 and S3.

Published OnlineFirst December 26, 2017; DOI: 10.1158/0008-5472.CAN-17-1833

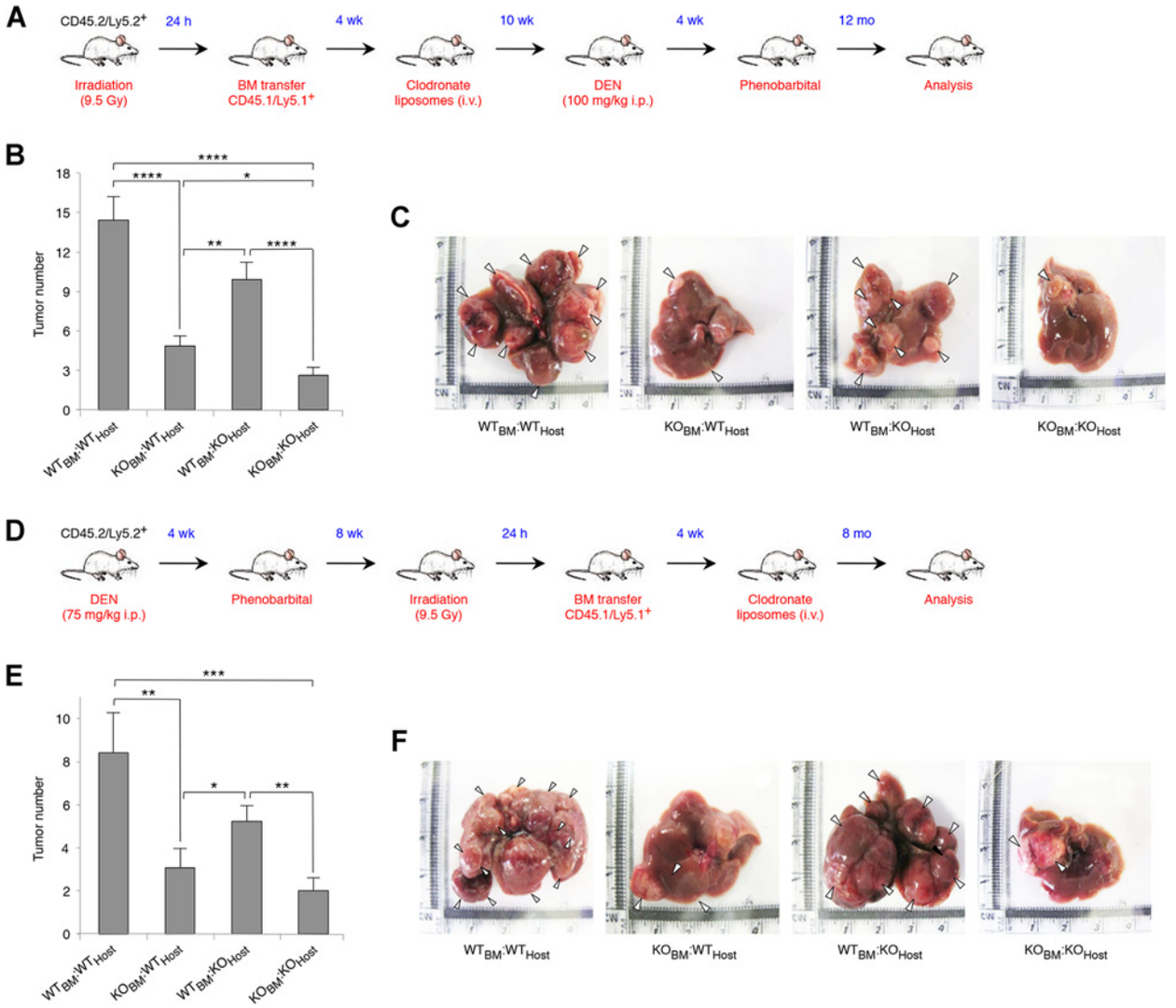

Figure 4.

Reduction of DEN-induced HCC development by *Gadd45b* deletion in bone marrow–derived cells. **A,** Summary of the treatment schedule used for Protocol A. **B,** Numbers of tumors (≥0.5 mm) in livers of WT_{BM}:WT_{Host} ($n = 40$), KO_{BM}:KO_{Host} ($n = 25$), KO_{BM}:WT_{Host} ($n = 36$), and WT_{BM}:KO_{Host} ($n = 35$) bone marrow chimeras at the time shown in **A**. **C,** Gross liver morphology in representative mice from **B**. **D,** Summary of the treatment schedule used for Protocol B. **E,** Numbers of tumors (≥0.5 mm) in livers of WT_{BM}:WT_{Host} ($n = 24$), KO_{BM}:KO_{Host} ($n = 23$), KO_{BM}:WT_{Host} ($n = 24$), and WT_{BM}:KO_{Host} ($n = 29$) bone marrow chimeras at the time shown in **D**. **F,** Gross liver morphology in representative mice from **E**. **A–F,** WT, *Gadd45b*$^{+/+}$; KO, *Gadd45b*$^{-/-}$. Bone marrow chimeras are identified as per "bone marrow donor:recipient" genotypes. **B** and **E,** Values, means ± SEM. *, $P < 0.05$; **, $P < 0.01$; ***, $P < 0.001$; ****, $P < 0.0001$. **C** and **F,** Arrowheads, tumors. Also, see Supplementary Fig. S4.

WT_{Host}; also compare KO_{BM}:WT_{Host} with KO_{BM}:KO_{Host}). In contrast, selective *Gadd45b* deletion in the hepatic parenchyma did not significantly affect HCC burden (compare WT_{BM}:KO_{Host} with WT_{BM}:WT_{Host}). In keeping with these findings, the additional *Gadd45b* ablation in bone marrow–derived cells did result in a significant reduction in tumor numbers in *Gadd45b*$^{-/-}$ hosts (compare WT_{BM}:KO_{Host} with KO_{BM}:KO_{Host}). Hence, selective *Gadd45b* loss in hematopoietic-derived cells is sufficient on its own to fully recapitulate the phenotype of *Gadd45b*$^{-/-}$ mice in DEN-induced carcinogenesis. We concluded that GADD45β promotes this oncogenic process largely by operating within immune and inflammatory cells.

Gadd45b loss hinders HCC progression

Given that the effect of *Gadd45b* loss on DEN-induced carcinogenesis intensifies in a tumor initiation–promotion model (Fig. 4B and C), is associated with increased TME-based inflammation (Figs. 2G–J and 3A–F; Supplementary Fig. S2A–S2E), and does not affect the acute hepatocyte proliferative response to DEN (Supplementary Fig. S3G and S3H), we hypothesized that GADD45β contributes to HCC progression, rather than initiation. As part of so-called "Protocol B" (Fig. 4D), mice of both genotypes were first challenged with DEN and placed on treatment with phenobarbital, and then adoptively transferred with *Gadd45b*$^{-/-}$ or *Gadd45b*$^{+/+}$ bone marrow, followed by Kupffer cell depletion,

Published OnlineFirst December 26, 2017; DOI: 10.1158/0008-5472.CAN-17-1833

as for Protocol A. Because, the *Gadd45b* status of inflammatory cells is modified 3 months after DEN injection, when preneoplastic foci have already largely progressed to HCCs (40), we reasoned that Protocol B would allow to distinguish between roles of GADD45β in tumor progression versus roles in tumor initiation.

Successful bone marrow–cell engraftment and Kupffer cell liver repopulation with donor-derived cells were verified as for Protocol A (Supplementary Fig. S4D and S4E). As expected, 12 months after DEN injection, the ratio between HCC numbers of isogenic *Gadd45b*$^{+/+}$ and *Gadd45b*$^{-/-}$ mice was similar to that observed with Protocol A (Fig. 4E and F; compare KO_{BM}:KO_{Host} with WT_{BM}:WT_{Host}; see also Fig. 4B and C). Strikingly, even when introduced after tumor initiation had already largely occurred in *Gadd45b*$^{+/+}$ livers, bone marrow–derived cell-specific *Gadd45b* ablation retained a virtually intact capacity to diminish oncogenesis (Fig. 4E; compare KO_{BM}:WT_{Host} with WT_{BM}:WT_{Host}). Accordingly, concomitant *Gadd45b* ablation in the hepatic parenchyma had no additional effect on HCC burden (compare KO_{BM}:WT_{Host} with KO_{BM}:KO_{Host}). Reciprocally, the introduction of *Gadd45b*$^{+/+}$ bone marrow into *Gadd45b*$^{-/-}$ hosts, 3 months after DEN injection, was still effective in restoring oncogenesis (compare WT_{BM}:KO_{Host} with KO_{BM}:KO_{Host}). Notably, these results were broadly equivalent to those obtained with Protocol A (see Fig. 4B). Collectively, these findings reinforce the conclusions that the GADD45β oncogenic function in DEN-induced tumorigenesis is largely restricted to the hematopoietic system and impacts upon tumor progression, while likely having little impact upon tumor initiation.

TME-associated *Gadd45b* loss in fibrosarcoma augments TAM infiltration and proinflammatory activation, while reducing tumor growth

To clarify the basis for the tumor-promoting activity of GADD45β in the TME and its significance in the association between *GADD45B* expression and aggressive disease pathology across human cancer types (Figs. 1A–M), we sought to investigate other model systems of established neoplasia, in which IKK/NF-κB drives oncogenesis by operating in immunoinflammatory cells. We reasoned that this approach could additionally clarify the basis for the oncogenic function of IKK/NF-κB itself in these cells. Indeed, although IKK/NF-κB inhibition in different epithelial cell types was shown to have discordant outcomes on oncogenesis, this inhibition in inflammatory cells, especially those of the myeloid lineage, has invariably resulted in oncogenesis suppression (16). We chose an initiated fibrosarcoma model in which hematopoietic cell–specific NF-κB1/p105 ablation was shown to augment TME-based inflammation and proinflammatory TAM activation, resulting in diminished tumor growth (19). As expected, subcutaneously implanted MCA-203 fibrosarcomas grew rapidly in immunocompetent C57BL76J *Gadd45b*$^{+/+}$ mice (Fig. 5A). Notably, however, tumor growth was markedly reduced in *Gadd45b*$^{-/-}$ hosts, thereby confirming in a different model system the essential oncogenic role of GADD45β in the TME.

As seen with HCC (Figs. 2I and J and 3A–D), the *Gadd45b*$^{-/-}$ TME contained a higher number of TAMs than the *Gadd45b*$^{+/+}$ TME (Fig. 5B; Supplementary Fig. S5A). Fibrosarcomas from *Gadd45b*$^{-/-}$ mice also contained more T cells than tumors from *Gadd45b*$^{+/+}$ hosts, although at the early time point examined (i.e., d19), this T-cell increase had not reached statistical significance (Figs. 5B; Supplementary Fig. S5A). Plausibly, this reflected the rapid evolution of fibrosarcoma allografts relative to endogenous DEN-induced HCCs and the delayed onset of adaptive relative to innate immune reactions (see also Figs. 2I and J). Indeed, the depletion of cytotoxic $CD8^+$ T cells by the use of a CD8-specific antibody resulted in a marked increase in fibrosarcoma growth, completely ablating any inhibitory effect of *Gadd45b* loss on oncogenesis (Fig. 5C and D; Supplementary Fig. S5B; compare tumor growth in *Gadd45b*$^{-/-}$ mice treated with anti-CD8 vs. control antibody; also note the similar tumor growth in *Gadd45b*$^{-/-}$ and *Gadd45b*$^{+/+}$ mice treated with the anti-CD8 antibody; see also Supplementary Fig. S5C). These data unequivocally demonstrate the critical importance of cytotoxic $CD8^+$ T cells in the antitumor effect of TME-associated *Gadd45b* loss. In contrast, TME-infiltrating B cells and granulocytes were unaffected by *Gadd45b* loss.

Underscoring the significance of the effects of GADD45β on TAMs, these cells comprised the major cellular component of the immunoinflammatory infiltrate in the *Gadd45b*$^{-/-}$ TME. Strikingly, the *Gadd45b*$^{-/-}$ TME also contained an approximately 4-fold higher number of TAMs expressing the proinflammatory markers, iNOS and COX-2 (14), than the *Gadd45b*$^{+/+}$ TME (Figs. 5E; Supplementary Fig. S5D). Reciprocally, fibrosarcomas from *Gadd45b*$^{-/-}$ mice displayed a lower number of Ym-1/$Chi3l3^+$ TAMs than tumors from *Gadd45b*$^{+/+}$ mice. Other anti-inflammatory activation markers were instead unaffected by *Gadd45b* loss (14). Hence, TME-associated *Gadd45b* ablation augments TAM infiltration, proinflammatory TAM activation, and $CD8^+$ T-cell–driven antitumor immune responses in fibrosarcoma, thus reinforcing our findings with DEN-induced HCC.

TME-specific *Gadd45b* loss augments proinflammatory TAM activation and intratumoral T-cell infiltration, while reducing ovarian oncogenesis

To further understand the general significance of GADD45β in TAM activation and malignant progression, we examined a third cancer model in which IKK/NF-κB was shown to drive oncogenesis by operating in myelomonocytic cells. We used ID8-Luc ovarian adenocarcinoma allografts because previous studies had shown that macrophage-specific IKKβ inhibition in this model reverses the typical anti-inflammatory TAM phenotype and enhances proinflammatory TAM activation, thereby causing tumor regression (18). Consistently, whereas syngeneic ID8-Luc tumors grew rapidly in the peritoneum of *Gadd45b*$^{+/+}$ mice, tumor growth was markedly reduced in *Gadd45b*$^{-/-}$ mice (Figs. 5F and G), thus demonstrating that TME-specific *Gadd45b* ablation also curbs ovarian oncogenesis.

Notably, intratumoral leukocyte infiltrates yielded a higher number of TAMs, T cells and granulocytes, but not B cells, in *Gadd45b*$^{-/-}$ compared with *Gadd45b*$^{+/+}$ mice (Fig. 5H). Significantly, as seen in DEN-induced HCC (Figs. 2I and J), the relative T-cell abundance in the *Gadd45b*$^{-/-}$ TME was largely due to an increased influx of $CD8^+$ cytotoxic T cells, which drive effective antitumor immune reactions (Fig. 5H; refs. 3, 5), rather than $CD4^+$ T cells. Consistent with the increased immunoreactivity of the *Gadd45b*$^{-/-}$ TME, a larger proportion of *Gadd45b*$^{-/-}$ than *Gadd45b*$^{+/+}$ TAMs expressed high surface levels of MHC-II (Fig. 5I and J; Supplementary Fig. S5E). Purified *Gadd45b*$^{-/-}$ TAMs also expressed higher levels of other proinflammatory genes, including *Nos2*, *Cxcl9*, *Cxcl10*, *Tnfa*, and *Il6*, than *Gadd45b*$^{+/+}$ TAMs, whereas anti-inflammatory activation genes, with the exception of *Ym-1/Chi3l3*, were unaffected by *Gadd45b* loss (Fig. 5K;

Published OnlineFirst December 26, 2017; DOI: 10.1158/0008-5472.CAN-17-1833

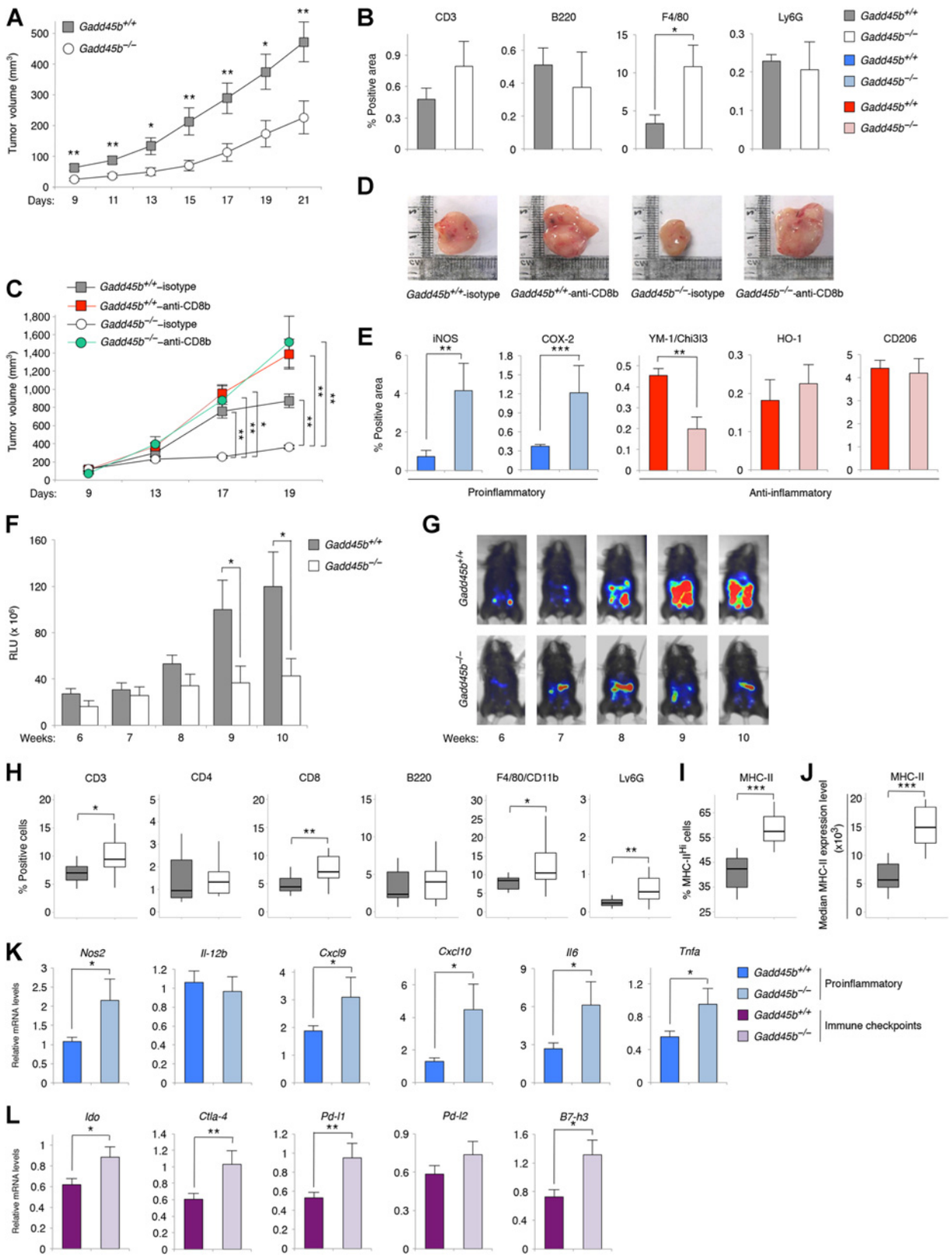

Published OnlineFirst December 26, 2017; DOI: 10.1158/0008-5472.CAN-17-1833

Supplementary Fig. S5F; ref. 14). In keeping with their heightened state of immune activation, *Gadd45b*$^{-/-}$ TAMs additionally expressed higher levels of immune checkpoint molecule-encoding genes, for example, *Ido*, *Ctla-4*, *Pd-l1*, and *B7-h3* (Fig. 5L; refs. 3, 4), thus confirming the observations made with DEN-induced HCC (Fig. 3E and F). Hence, in three distinct models of solid cancer, TME-specific *Gadd45b* ablation increased proinflammatory TAM activation, and intratumoral macrophage and CD8$^+$ T-cell infiltration (see also Figs. 2G–J, 3A–F, 5B, E, and H–L; Supplementary Figs. S2E; S5A, S5D, and S5E), resulting in diminished tumor growth. Interestingly, these effects of *Gadd45b* loss on oncogenesis phenocopied the effects of myeloid-specific IKKβ/NF-κB inhibition (16, 18, 19). Collectively, these findings underpin the importance of the TME-specific role of GADD45β in curbing tumor-associated inflammation and immune infiltration across different cancer types.

Gadd45b loss promotes proinflammatory macrophage activation via a cell-autonomous mechanism

We sought to investigate whether GADD45β mediated its effects on TAM activation via a cell-autonomous mechanism. We used an *ex vivo* coculture model system mimicking the tumor cell/macrophage interactions occurring in cancer, *in vivo* (18). Consistent with our *in vivo* findings (Figs. 5E; Supplementary Fig. S5D), upon coculture with MCA-203 cells, *Gadd45b*$^{-/-}$ BMDMs expressed markedly higher levels of proinflammatory M1-like genes, including *Nos2*, *Tnfa*, and *Cxcl10*, and lower levels of *Arg-1*, but not of other anti-inflammatory M2-like genes, than *Gadd45b*$^{+/+}$ BMDMs (Fig. 6A). Similar results were obtained when *Gadd45b*$^{-/-}$ and *Gadd45b*$^{+/+}$ BMDMs were cocultured under similar conditions with ID8-Luc carcinoma cells (Supplementary Fig. S6A; see also Figs. 5I–K; Supplementary Fig. S5F). Hence, GADD45β plays an essential and cell-autonomous role in restraining proinflammatory macrophage activation in response to cues from tumor cells.

To clarify the mechanisms by which GADD45β governs tumor cell–induced macrophage activation, we used a tumor cell–free model system, which employs cytokines and TLR ligands to polarize macrophages (7, 8). As expected, proinflammatory M1-like genes, as well as known NF-κB target genes, including *Gadd45b*, *Nfkbia*, and *Tnfaip3*, were strongly upregulated by IFNγ and lipopolysaccharide (LPS) in *Gadd45b*$^{+/+}$ BMDMs (Fig. 6B). Each of the proinflammatory M1-like genes tested, however, was further significantly upregulated in IFNγ/LPS-treated *Gadd45b*$^{-/-}$ BMDMs compared with *Gadd45b*$^{+/+}$ BMDMs. Immune checkpoint molecule-coding genes, including *Ido* and *Pd-l2*, were also markedly increased in IFNγ/LPS-stimulated *Gadd45b*$^{-/-}$ BMDMs relative to controls (Fig. 6B), in keeping with our *in vivo* findings (Figs. 3E and F and 5L). In contrast, *Gadd45b* expression was unaffected by treatment with IL4 and IL13, as was the upregulation of each of the anti-inflammatory M2-like genes analyzed (Fig. 6C). We concluded that GADD45β is required to curb inflammation and M1-like macrophage activation, but is not directly involved in anti-inflammatory M2-like polarization, suggesting that the perturbation of the anti-inflammatory activation profile of *Gadd45b*$^{-/-}$ TAMs, occasionally observed in coculture systems and *in vivo*, stemmed from the skewing of these cells toward a proinflammatory activation phenotype. Collectively, these findings provide a mechanism for the effect of *Gadd45b* loss on tumor-associated inflammation and proinflammatory TAM polarization, *in vivo*.

Gadd45b loss exacerbates proinflammatory M1-like polarization by enhancing p38 signaling

To further the mechanistic understanding of the role of GADD45β in macrophage polarization, we examined STAT1 and MAPK signaling, which upregulates the M1-like activation program downstream of IFNγ receptor (IFNγR) and TLRs (41). As shown in Fig. 6D and E, stimulation with IFNγ and LPS activated these pathways, as well as GADD45β expression, in *Gadd45b*$^{+/+}$ BMDMs. Yet, *Gadd45b* deletion had no effect on either STAT1 or ERK phosphorylation, nor did it have any effect on JNK signaling, nor on NF-κB activation (Fig. 6D and E). Surprisingly, *Gadd45b* loss instead markedly augmented and prolonged IFNγ/LPS-induced p38 signaling, at each of the time points examined (Fig. 6D). We concluded that GADD45β is required to restrict both the magnitude and duration of p38 activation during proinflammatory macrophage polarization.

Because p38 governs inflammation and expression of many of the proinflammatory M1-denoting genes deregulated by *Gadd45b* loss (42), we hypothesized that GADD45β inhibits proinflammatory macrophage polarization by restraining exacerbated p38 signaling. We therefore investigated whether attenuating this signaling reversed the effects of *Gadd45b* loss on macrophage activation. Notably, treatment with the specific

Figure 5.

Increased intratumoral immunoinflammatory infiltration, proinflammatory TAM activation, and reduced fibrosarcoma and ovarian carcinoma growth in *Gadd45b*$^{-/-}$ mice. **A,** Volumes of subcutaneous MCA-203 fibrosarcoma allografts in *Gadd45b*$^{+/+}$ ($n = 10$) and *Gadd45b*$^{-/-}$ ($n = 9$) mice at the times shown. **B,** IHC analysis showing the percentage of positive areas per field at ×400 of the indicated immune cell populations in MCA-203 tumors from *Gadd45b*$^{+/+}$ ($n = 7$) and *Gadd45b*$^{-/-}$ ($n = 8$) mice 19 days after tumor cell injection. **C,** Volumes of subcutaneous MCA-203 fibrosarcoma allografts in *Gadd45b*$^{+/+}$ and *Gadd45b*$^{-/-}$ mice treated with anti-CD8 or isotype control antibody, as shown, at the times indicated. *Gadd45b*$^{+/+}$: anti-CD8 ($n = 9$), isotype ($n = 7$); *Gadd45b*$^{-/-}$: anti-CD8 ($n = 9$), isotype ($n = 4$). **D,** Images of representative tumors from **C** at day 20. **E,** IHC analysis showing the percentage of positive areas per field at ×400 of the indicated proinflammatory and anti-inflammatory activation markers in the tumors from **B**. **F,** Relative luminescence units (RLU) of intraperitoneal ID8-Luc ovarian tumor allografts in *Gadd45b*$^{+/+}$ ($n = 10$) and *Gadd45b*$^{-/-}$ ($n = 10$) mice at the times shown after tumor cell injection. **G,** Bioluminescence images of representative mice from **F** presented as a pseudocolor scale, whereby red and blue denote the highest and lowest photon flux, respectively. **H,** FACS analysis showing the percentage of the indicated intratumoral immune cell populations in *Gadd45b*$^{+/+}$ ($n = 12$) and *Gadd45b*$^{-/-}$ ($n = 13$) mice 60 days after ID8-Luc tumor cell injection. **I,** FACS analysis showing the percentage of CD11b$^+$ and F4/80$^+$ double positive TAMs expressing high MHC-II levels (MHC-II^{high}) in ID8-Luc tumors from **H**. **J,** FACS analysis showing the median MHC-II fluorescence intensity of CD11b$^+$ and F4/80$^+$ double positive TAMs in ID8-Luc tumors from **H**. **H–J,** Boxes span between the highest values of the first and third quartiles; whiskers extend to the highest and lowest values within 1.5× of the interquartile range. Lines within boxes, medians. **K** and **L,** qRT-PCR showing the relative mRNA levels of the indicated proinflammatory activation markers (**K**) and immune checkpoint molecules (**L**) in CD11b$^+$ TAMs from *Gadd45b*$^{+/+}$ ($n = 22$) and *Gadd45b*$^{-/-}$ ($n = 10$ or $n = 12$) mice 10 weeks after ID8-Luc cell injection. **A–C**, **E**, **F**, **K**, and **L,** Values, means ± SEM. **A–C**, **E**, **F**, and **H–L,** *, $P < 0.05$; **, $P < 0.01$; ***, $P < 0.001$. Also, see Supplementary Fig. S5.

Published OnlineFirst December 26, 2017; DOI: 10.1158/0008-5472.CAN-17-1833

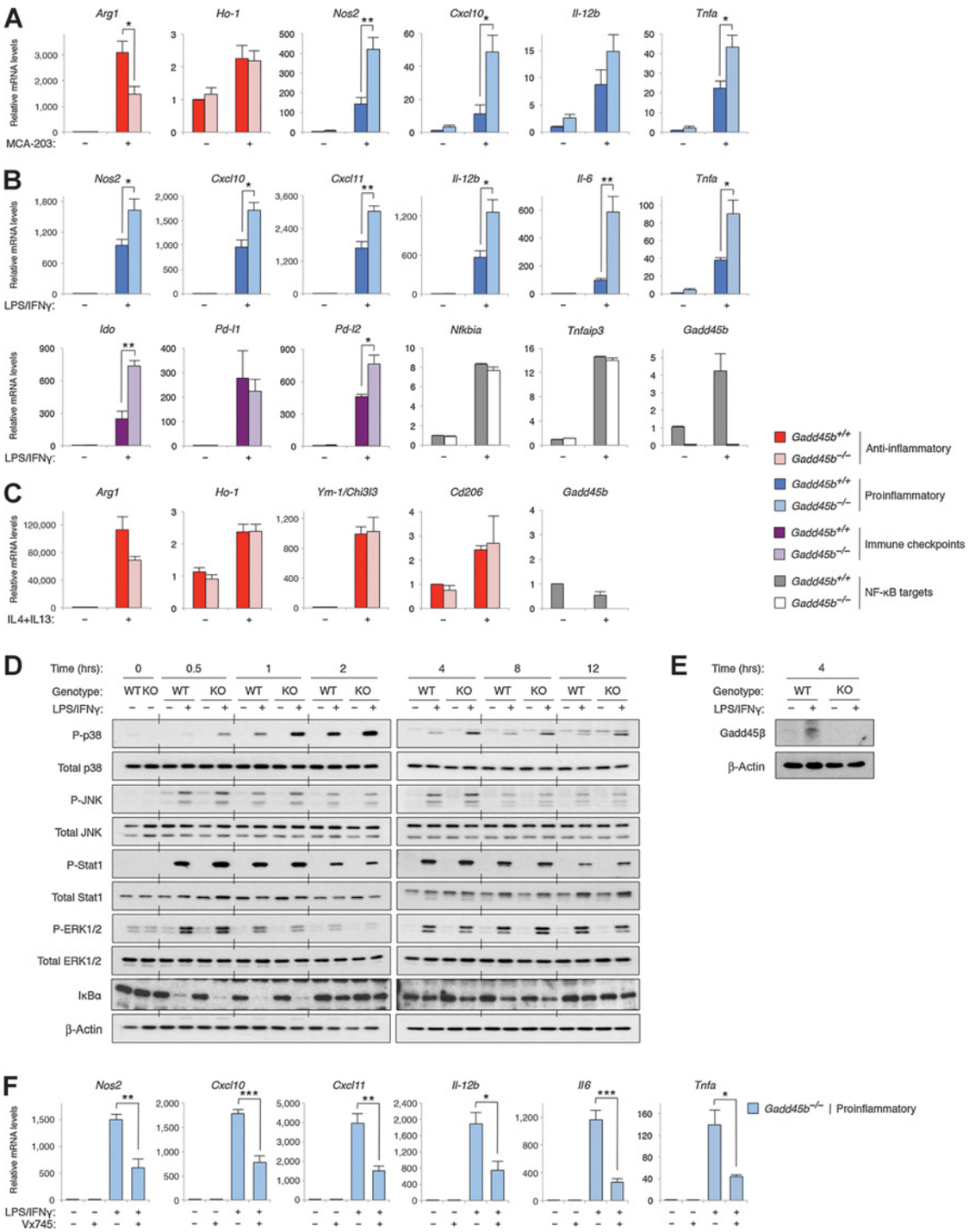

Figure 6.

Gadd45b loss increases proinflammatory macrophage activation by enhancing p38 signaling. **A,** qRT-PCR showing the relative mRNA levels of the indicated proinflammatory and anti-inflammatory genes in BMDMs from *Gadd45b*$^{+/+}$ and *Gadd45b*$^{-/-}$ mice after a 24-hour coculture with MCA-203 cells. **B,** qRT-PCR showing the relative mRNA levels of the indicated proinflammatory, NF-κB–regulated and immune checkpoint molecule-coding genes in BMDMs from *Gadd45b*$^{-/-}$ and *Gadd45b*$^{+/+}$ mice after a 4-hour (*Nfkbia, Tnfaip3*, and *Gadd45b*) or 12-hour (all other genes) stimulation with LPS and IFNγ. **C,** qRT-PCR showing the relative mRNA levels of the indicated anti-inflammatory genes after a 26-hour stimulation with IL4 and IL13. **D** and **E,** Western blots showing total and phosphorylated (P) proteins in *Gadd45b*$^{+/+}$ and *Gadd45b*$^{-/-}$ BMDMs after stimulation with LPS and IFNγ for the times indicated. β-Actin is shown as loading control. **F,** qRT-PCR showing the relative mRNA levels of the indicated proinflammatory genes in *Gadd45b*$^{-/-}$ BMDMs left untreated (−) or treated with LPS and IFNγ (+) for 12 hours in the presence (+) or absence (−) of the p38 inhibitor, Vx745 (20 μmol/L). **A–C** and **F,** Values, means ± SEM [**A**, **B** (top), and **F**, $n = 4$; **B** (bottom) and **C**, $n = 3$]. *, $P < 0.05$; **, $P < 0.01$; ***, $P < 0.001$. Also, see Supplementary Fig. S6.

Published OnlineFirst December 26, 2017; DOI: 10.1158/0008-5472.CAN-17-1833

p38α/β inhibitor, Vx745 (http://www.kinase-screen.mrc.ac.uk/screening-compounds/348786), downregulated the IFNγ/LPS–dependent induction of each of the proinflammatory M1-like genes that were overactivated by *Gadd45b* loss to levels similar to those observed in IFNγ/LPS–stimulated *Gadd45b*$^{+/+}$ BMDMs (Fig. 6F; see also Fig. 6B). Comparable results were obtained using two additional, structurally unrelated p38 inhibitors, that is, skepinone-L and SB203580, thus excluding any off-target effect of Vx745 (Supplementary Fig. S6B and S6C). We concluded that GADD45β suppresses proinflammatory macrophage activation by selectively downregulating IFNγ/LPS–induced p38 signaling.

Macrophage-specific *Gadd45b* loss is sufficient to diminish oncogenesis

To clarify the cause–effect relationship between macrophage-specific *Gadd45b* deficiency and oncogenesis suppression, we generated mice carrying homozygous loxP-flanked *Gadd45b* alleles (*Gadd45b*$^{F/F}$ mice; Fig. 7A; Supplementary Fig. S7A and S7B), and crossed them with *LysM-cre* transgenic mice to obtain myeloid-specific *Gadd45b*-null mice (*Gadd45b*$^{\Delta M/\Delta M}$), after Cre-mediated recombination (Supplementary Fig. S7C; ref. 33). PCR analyses confirmed the selective excision of the *Gadd45b*^{F} alleles and the resulting ablation of *Gadd45b* mRNA expression in *Gadd45b*$^{\Delta M/\Delta M}$ splenic macrophages, but not splenic B or T lymphocytes (Fig. 7B and C).

Given that the *LysM-cre* transgene, which efficiently deletes loxP-targeted alleles in circulating myelomonocytic cells, is not useful in Kupffer cells (33), *Gadd45b*$^{\Delta M/\Delta M}$ mice could not be tested in the DEN HCC model. We therefore used them in the context of MCA-203 fibrosarcoma allografts. As expected, MCA-203 tumor growth was unaffected by the presence of *Gadd45b*$^{F/F}$ alleles (Fig. 7D and E; see also Fig. 5A). Strikingly, however, this growth was markedly diminished in *Gadd45b*$^{\Delta M/\Delta M}$ mice to a similar extent as seen in *Gadd45b*$^{-/-}$ mice (Fig. 7D and E; see Fig. 5A), indicating that macrophage-specific *Gadd45b* loss is sufficient on its own to fully recapitulate the effect of complete TME-based *Gadd45b* deficiency on inflammation-driven oncogenesis.

We sought to confirm this macrophage-specific role of GADD45β in oncogenesis by using an alternative mouse model. To this end, ID8-Luc ovarian tumors were allowed to grow in *Gadd45b*$^{+/+}$ mice until they became detectable by bioimaging, at which point, mice were adoptively transferred with *ex vivo* cultured *Gadd45b*$^{+/+}$ or *Gadd45b*$^{-/-}$ BMDMs (0 week; Figs. 7F–H). As expected, following *Gadd45b*$^{+/+}$ BMDM transfer, ovarian tumors continued to grow rapidly (Figs. 7G and H). In contrast, the transfer of *Gadd45b*$^{-/-}$ BMDMs resulted in a significant inhibition of tumor growth. As seen with fibrosarcoma (Figs. 7D and E), the effects of macrophage-specific *Gadd45b* loss on ovarian carcinogenesis recapitulated the tumor-suppressive effect of complete TME-based *Gadd45b* ablation (Figs. 5F and G). Together with our findings with *Gadd45b*$^{\Delta M/\Delta M}$ mice, these results demonstrate that GADD45β orchestrates the tumor-promoting activity of the TME across multiple cancer types by operating in myeloid cells. Collectively, our findings provide a mechanism for the immunosuppressive activity of the TME that restricts tumor-based inflammation and CD8$^+$ T-cell trafficking into tumors and underscore the general significance of the NF-κB–dependent mechanisms mediated by GADD45β in human malignant disease.

Discussion

We have identified an essential innate immunity "checkpoint" governed by the GADD45β-dependent axis of the NF-κB pathway that counters TME-based inflammation and CD8$^+$ T-cell trafficking into tumors, the major barrier to effective anticancer immunotherapy (3, 5). In three distinct models of cancers that are largely refractory to immunotherapies (43–45), myeloid-associated *Gadd45b* ablation restored proinflammatory TAM activation and intratumoral CD8$^+$ T-cell infiltration, leading to diminished tumor growth. These findings uncover a mechanism for the immunosuppressive activity of the TME that fosters oncogenesis. They also provide a basis for the anti-inflammatory role that IKKβ/NF-κB plays in the myeloid lineage and identify a candidate therapeutic route in the innate immune system for "reeducating" TAMs to overcome TME-mediated immunosuppression and, potentially, resistance to immunotherapies.

The treatment of certain malignancies is being revolutionized by the development of effective immunotherapies, such as antagonists of immune checkpoint molecules (4). Yet, the large majority of patients fail to respond to these treatments, due to the presence of additional immunoinhibitory mechanisms in the TME that prevent T-cell access into tumors or cause T-cell exhaustion (3, 5). However, the limited understanding of these mechanisms currently precludes the development of effective treatment strategies for breaking the TME-mediated resistance to immunotherapies. An attractive approach to overcome this resistance would be to harness the innate immune system to induce tumor-based inflammation and CD8$^+$ T-cell entry and expansion in the TME. Together, the myeloid-specific role of IKKβ/NF-κB in suppressing proinflammatory TAM activation (15) and the central role of myeloid cells in cancer immune evasion (6, 7) provide a compelling rationale for therapeutically targeting IKKβ/NF-κB signaling to reprogram TAMs toward a proinflammatory activation phenotype capable of eliciting local antitumor immune responses (18, 19). Yet, no specific IKKβ/NF-κB inhibitor has so far been clinically approved.

Our finding that GADD45β mediates an essential innate immunoinhibitory mechanism therefore provides an attractive route downstream in the IKKβ/NF-κB pathway to redirect CD8$^+$ T-cell trafficking into tumors and reactivate silenced CD8$^+$ T-cell–driven antitumor immune responses. Congruently, in various cancer types, selective GADD45β ablation in myelomonocytic cells closely phenocopied the effects of IKKβ/NF-κB inactivation on oncogenesis (15, 16, 18, 19). Importantly, myeloid-specific GADD45β deletion appeared to override TME-mediated CD8$^+$ T-cell exclusion, plausibly through a mechanism involving the upregulation of CXCR3-binding chemokines, for example, CXCL9, CXCL10, and CXCL11, which recruit Th-1–type and CD8$^+$ effector T cells into tumors and extranodal sites of inflammation (5, 46). Underscoring the importance of the GADD45β-mediated function, the depletion of CD8$^+$ T cells completed abrogated any effect of myeloid-restricted *Gadd45b* loss on oncogenesis. Indeed, GADD45β blockade appeared to also enhance the ability of the TME to support T-cell effector functions by upregulating multiple inflammatory mediators, proinflammatory TAM functionalities, and MHC-II molecules. Underscoring the coordinated nature of its multiple effects on the immune system, GADD45β ablation further imparted anatomic organization to adaptive immune reactions, enabling them to assemble into well-configured TLSs within endogenously arisen tumors.

Published OnlineFirst December 26, 2017; DOI: 10.1158/0008-5472.CAN-17-1833

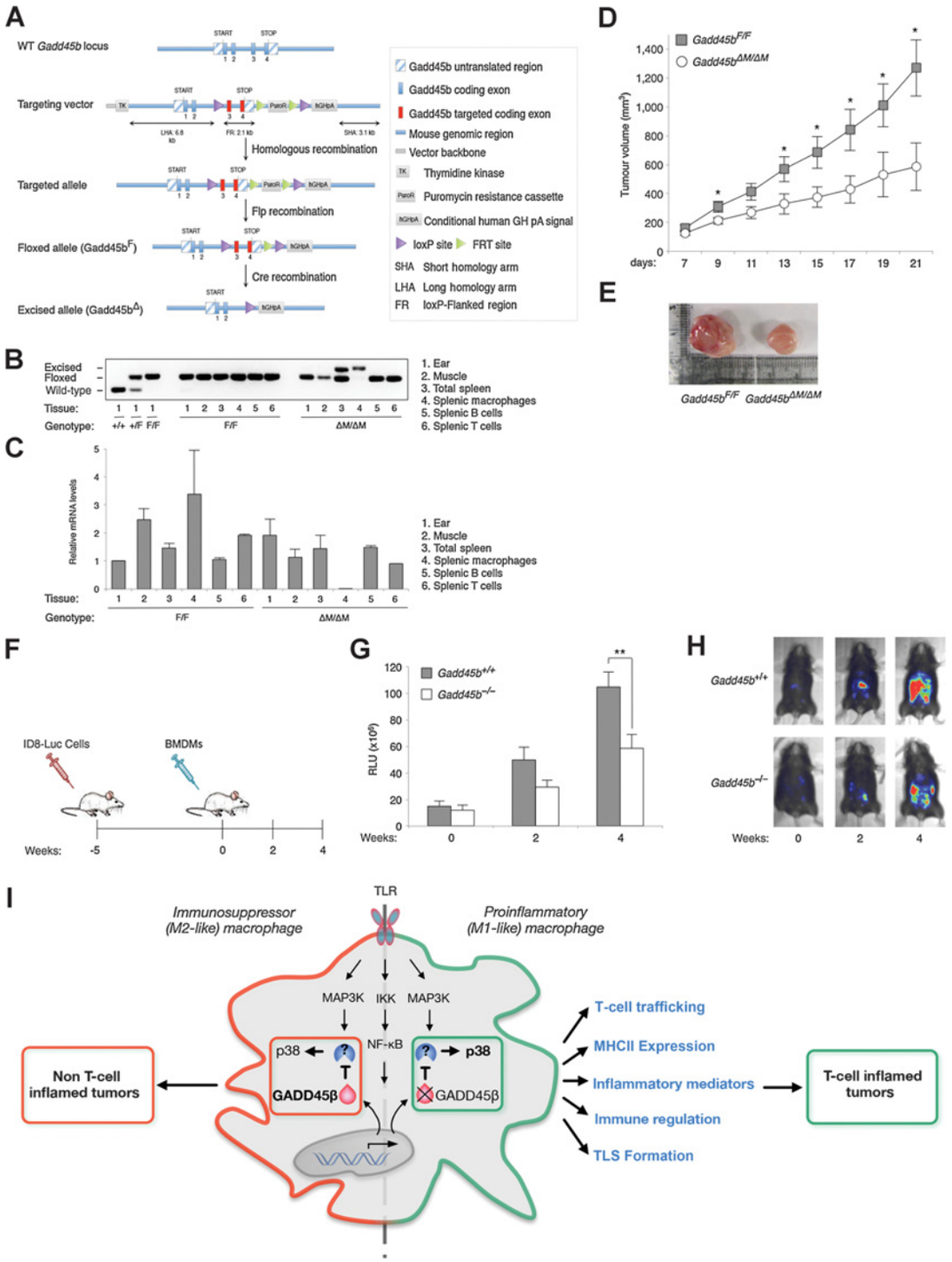

Figure 7.

Suppression of oncogenesis by macrophage-specific *Gadd45b* deletion. **A,** The targeting strategy for generating the loxP-flanked *Gadd45b* allele (*Gadd45b*^{F}). **B,** PCR detecting the wild-type (*Gadd45b*$^{+}$), *Gadd45b*^{F}, or excised (*Gadd45b*$^{\Delta}$) *Gadd45b* alleles in the indicated tissues from *Gadd45b*$^{+/+}$ ($^{+/+}$), *Gadd45b*$^{+/F}$ ($^{+/F}$), *Gadd45b*$^{F/F}$ ($^{F/F}$), or *Gadd45b*$^{F/F}$;*LysM-cre* ($^{\Delta M/\Delta M}$) mice. **C,** qRT-PCR showing the relative *Gadd45b* mRNA levels in the indicated tissues isolated from *Gadd45b*$^{F/F}$ ($^{F/F}$) or *Gadd45b*$^{F/F}$;*LysM-cre* ($^{\Delta M/\Delta M}$) mice. **D,** Volumes of subcutaneous MCA-203 fibrosarcoma allografts in *Gadd45b*$^{\Delta M/\Delta M}$ ($n = 9$) and *Gadd45b*$^{F/F}$ ($n = 8$) mice at the times shown. **E,** Images of representative tumors from **D** at day 21. **F,** Summary of the cell injection schedule used in **G** and **H**. **G,** Relative luminescence units (RLU) of intraperitoneal ID8-Luc ovarian tumor allografts in *Gadd45b*$^{+/+}$ mice at the times indicated after intraperitoneal injection of *Gadd45b*$^{+/+}$ ($n = 9$) or *Gadd45b*$^{-/-}$ ($n = 12$) BMDM pools. **H,** Bioluminescence images of representative mice from **G** presented as a pseudocolor scale as in Fig. 5G. **I,** Schematic representation of the oncogenic function of GADD45β in macrophages. **C**, **D**, and **G,** Values, means ± SEM. *, $P < 0.05$; **, $P < 0.01$. Also, see Supplementary Fig. S7.

Published OnlineFirst December 26, 2017; DOI: 10.1158/0008-5472.CAN-17-1833

Although Pikarsky and colleagues recently suggested that TLSs facilitate HCC initiation and early promotion, their study investigated TLS formation in the context of the preneoplastic hepatic parenchyma and inflamed neoplastic liver outside HCCs (47). Indeed, T- and B-cell immunity has been previously shown to counter DEN-induced HCC development in mouse models (47, 48), and intratumoral TLSs have been shown to portend a favorable clinical outcome in the majority of human cancers, including HCC (37, 49). Future studies will determine the precise mechanisms by which GADD45β curbs TME-based TLS formation and cytotoxic $CD8^+$ T-cell trafficking and activation, as well as how these mechanisms relate to the GADD45β-mediated anti-inflammatory function in myeloid cells. Irrespective of the mechanisms, the profound effects of *Gadd45b* loss on macrophage and T-cell accumulation in the TME and intratumoral TLS formation underscore the broad clinical potential of the GADD45β-dependent anti-inflammatory axis of the IKK/NF-κB pathway in anticancer immunotherapy.

Because GADD45β also serves as an essential NF-κB–regulated inhibitor of cancer cell apoptosis (24), our finding of its unexpected function in the innate immune system demonstrates that a single pivotal axis of the IKK/NF-κB pathway, that is, the GADD45β-dependent axis, integrates the oncogenic mechanism suppressing tumor cell apoptosis with the mechanism restraining TME-based inflammation and T-cell infiltration. Hence, GADD45β serves as a central downstream hub in the IKK/NF-κB pathway linking cancer and inflammation. Surprisingly, GADD45β appears to perform these oncogenic functions via separable, tissue-specific mechanisms, attenuating proinflammatory p38 signaling within TAMs to restrain proinflammatory activation, while inhibiting apoptosis of cancer cells by suppressing JNK/MKK7 signaling (Fig. 7I; ref. 24). Future studies will clarify the precise mechanism(s) by which GADD45β curbs p38 activation in myeloid cells and confirm the role of this mechanism in oncogenesis. Irrespective of these mechanism(s), our results postulate that targeting the IKKβ/NF-κB pathway through GADD45β inhibition provides a candidate therapeutic route to counter oncogenesis by reversing TME-mediated immunosuppression and, at the same time, inducing apoptosis of cancer cells, thereby affording dual clinical benefit. Indeed, a combination of oncogenic mechanisms mediated by GADD45β in malignant and TME-based myeloid cells likely underpins the correlations between elevated *GADD45B* expression and poor clinical outcome observed in the large majority of human cancers.

To circumvent the limitations of IKK/NF-κB–targeting agents, we recently adopted the strategy of therapeutically targeting a nonredundant, pathogenically critical axis of the NF-κB pathway, similarly mediated by GADD45β, in multiple myeloma, rather than NF-κB globally (24, 50). Initial results from the first-in-human clinical study of GADD45β/MKK7–targeting therapeutics in patients with multiple myeloma preliminarily indicate the clinical safety of these agents, alongside cancer-selective pharmacodynamic response (L. Tornatore and G. Franzoso, unpublished observations). These encouraging early clinical results suggest that it may be possible to similarly target the GADD45β-binding factor regulating p38 signaling in myeloid cells, to elicit antitumor inflammation. Notably, by converting tumors lacking a spontaneous $CD8^+$ T-cell infiltrate into $CD8^+$ T-cell–infiltrated tumors and, concurrently, upregulating immune checkpoint molecules, for example, IDO and PD-1 ligands, innate immunotherapies targeting GADD45β could conceivably overcome primary resistance to adaptive immunotherapies, and thereby increase response rates in currently recalcitrant cancer patient subsets (3, 5).

Further studies will clarify the clinical benefit of combining GADD45β inhibitors with conventional immunotherapies. Notwithstanding, the remarkable consistency of the effects of myeloid-specific *Gadd45b* deletion on oncogenesis and the widespread correlation of *GADD45B* expression with aggressive disease pathology across most human cancer types underscore the general clinical significance of the GADD45β-mediated mechanism and, consequently, the potential of GADD45β-targeting therapeutics in human malignant disease. The new added focus provided by our current findings of a role of GADD45β in innate immune regulation will also invigorate the drug discovery effort to develop novel GADD45β-targeting immunotherapeutics for safely and effectively treating oncological diseases.

Disclosure of Potential Conflicts of Interest

No potential conflicts of interest were disclosed.

Authors' Contributions

Conception and design: D. Verzella, J. Bennett, M. Fischietti, A.K. Thotakura, E. Alesse, F. Zazzeroni, G. Franzoso

Development of methodology: D. Verzella, J. Bennett, M. Fischietti, A.K. Thotakura, C. Recordati, L. Tornatore, F. Zazzeroni, G. Franzoso

Acquisition of data (provided animals, acquired and managed patients, provided facilities, etc.): D. Verzella, J. Bennett, M. Fischietti, A.K. Thotakura, F. Pasqualini, D. Capece, D. Vecchiotti, B. Di Francesco, F. Begalli, L. Tornatore, S. Papa, S.J. Forbes, F. Zazzeroni

Analysis and interpretation of data (e.g., statistical analysis, biostatistics, computational analysis): J. Bennett, A.K. Thotakura, C. Recordati, D. D'Andrea, M. De Maglie, S. Papa, A. Sica, E. Alesse, F. Zazzeroni, G. Franzoso

Writing, review, and/or revision of the manuscript: D. Verzella, J. Bennett, M. Fischietti, A.K. Thotakura, C. Recordati, D. Capece, D. D'Andrea, F. Begalli, S. Papa, S.J. Forbes, E. Alesse, F. Zazzeroni, G. Franzoso

Administrative, technical, or material support (i.e., reporting or organizing data, constructing databases): J. Bennett, F. Pasqualini, T. Lawrence, A. Sica

Study supervision: F. Zazzeroni, G. Franzoso

Acknowledgments

The work was supported in part by Cancer Research UK programme grant A15115, Medical Research Council (MRC) Biomedical Catalyst grant MR/L005069/1 and Bloodwise project grant 15003 to G. Franzoso, the Associazione Italiana per la Ricerca sul Cancro (AIRC) grants 1432 and 5172 and MIUR PRIN grant no. 2009EWAW4M_003 to F. Zazzeroni, MIUR FIRB grant no. RBAP10A9H9 to E. Alesse, and the Associazione Italiana per la Ricerca sul Cancro (AIRC) grant 15585 to A. Sica. We thank N. van Rooijen for providing clodronate liposomes, I. Marigo and V. Bronte for providing the MCA-203 cell line, and J. Dyson for assistance with animal studies. We also thank V. Tybulewicz, A. Leonardi, G. Melino, and J. Behmoaras for critical reading of the manuscript. D. Verzella and B. Di Francesco were supported by the L'Aquila University PhD program in Experimental Medicine. M. Fischietti and D. Vecchiotti were supported by the L'Aquila University PhD program in Biotechnology.

The costs of publication of this article were defrayed in part by the payment of page charges. This article must therefore be hereby marked *advertisement* in accordance with 18 U.S.C. Section 1734 solely to indicate this fact.

Received June 22, 2017; revised November 20, 2017; accepted December 19, 2017; published OnlineFirst December 26, 2017.

Published OnlineFirst December 26, 2017; DOI: 10.1158/0008-5472.CAN-17-1833

References

1. Hanahan D, Weinberg RA. Hallmarks of cancer: the next generation. Cell 2011;144:646–74.
2. Grivennikov SI, Greten FR, Karin M. Immunity, inflammation, and cancer. Cell 2010;140:883–99.
3. Joyce JA, Fearon DT. T cell exclusion, immune privilege, and the tumor microenvironment. Science 2015;348:74–80.
4. Topalian SL, Drake CG, Pardoll DM. Immune checkpoint blockade: a common denominator approach to cancer therapy. Cancer Cell 2015;27:450–61.
5. Gajewski TF, Schreiber H, Fu YX. Innate and adaptive immune cells in the tumor microenvironment. Nat Immunol 2013;14:1014–22.
6. Noy R, Pollard JW. Tumor-associated macrophages: from mechanisms to therapy. Immunity 2014;41:49–61.
7. Biswas SK, Allavena P, Mantovani A. Tumor-associated macrophages: functional diversity, clinical significance, and open questions. Semin Immunopathol 2013;35:585–600.
8. Qian BZ, Pollard JW. Macrophage diversity enhances tumor progression and metastasis. Cell 2010;141:39–51.
9. Ries CH, Cannarile MA, Hoves S, Benz J, Wartha K, Runza V, et al. Targeting tumor-associated macrophages with anti-CSF-1R antibody reveals a strategy for cancer therapy. Cancer Cell 2014;25:846–59.
10. Zhu Y, Knolhoff BL, Meyer MA, Nywening TM, West BL, Luo J, et al. CSF1/CSF1R blockade reprograms tumor-infiltrating macrophages and improves response to T-cell checkpoint immunotherapy in pancreatic cancer models. Cancer Res 2014;74:5057–69.
11. Strachan DC, Ruffell B, Oei Y, Bissell MJ, Coussens LM, Daniel D. CSF1R inhibition delays cervical and mammary tumor growth in murine models by attenuating the turnover of tumor-associated macrophages and enhancing infiltration by CD8+ T cells. Oncoimmunology 2013;2:e26968.
12. Mitchem JB, Brennan DJ, Knolhoff BL, Belt BA, Zhu Y, Sanford DE, et al. Targeting tumor-infiltrating macrophages decreases tumor-initiating cells, relieves immunosuppression, and improves chemotherapeutic responses. Cancer Res 2013;73:1128–41.
13. DeNardo DG, Brennan DJ, Rexhepaj E, Ruffell B, Shiao SL, Madden SF, et al. Leukocyte complexity predicts breast cancer survival and functionally regulates response to chemotherapy. Cancer Discov 2011;1:54–67.
14. Sica A, Mantovani A. Macrophage plasticity and polarization: in vivo veritas. J Clin Invest 2012;122:787–95.
15. Lawrence T. Macrophages and NF-κB in cancer. Curr Topics Microbiol 2011;349:171–84.
16. Ben-Neriah Y, Karin M. Inflammation meets cancer, with NF-κB as the matchmaker. Nat Immunol 2011;12:715–23.
17. DiDonato JA, Mercurio F, Karin M. NF-κB and the link between inflammation and cancer. Immunol Rev 2012;246:379–400.
18. Hagemann T, Lawrence T, McNeish I, Charles KA, Kulbe H, Thompson RG, et al. "Re-educating" tumor-associated macrophages by targeting NF-κB. J Exp Med 2008;205:1261–8.
19. Saccani A, Schioppa T, Porta C, Biswas SK, Nebuloni M, Vago L, et al. p50 nuclear factor-kappaB overexpression in tumor-associated macrophages inhibits M1 inflammatory responses and antitumor resistance. Cancer Res 2006;66:11432–40.
20. Lawrence T, Fong C. The resolution of inflammation: anti-inflammatory roles for NF-kappaB. Int J Biochem Cell Biol 2010;42:519–23.
21. Lawrence T, Bebien M, Liu GY, Nizet V, Karin M. IKKalpha limits macrophage NF-kappaB activation and contributes to the resolution of inflammation. Nature 2005;434:1138–43.
22. Papa S, Zazzeroni F, Bubici C, Jayawardena S, Alvarez K, Matsuda S, et al. Gadd45 beta mediates the NF-kappa B suppression of JNK signalling by targeting MKK7/JNKK2. Nat. Cell Biol 2004;6:146–53.
23. De Smaele E, Zazzeroni F, Papa S, Nguyen DU, Jin R, Jones J, et al. Induction of gadd45beta by NF-kappaB downregulates pro-apoptotic JNK signalling. Nature 2001;414:308–13.
24. Tornatore L, Sandomenico A, Raimondo D, Low C, Rocci A, Tralau-Stewart C, et al. Cancer-selective targeting of the NF-κB survival pathway with GADD45β/MKK7 inhibitors. Cancer Cell 2014:26:495–508.
25. Tomczak K, Czerwinska P, Wiznerowicz M. The Cancer Genome Atlas (TCGA): an immeasurable source of knowledge. Contemp Oncol 2015;19:A68–A77.
26. Goldman M, Craft B, Swatloski T, Cline M, Morozova O, Diekhans M, et al. The UCSC cancer genomics browser: update 2015. Nucleic Acids Res 2015;43:D812–7.
27. Marisa L, de Reynies A, Duval A, Selves J, Gaub MP, Vescovo L, et al. Gene expression classification of colon cancer into molecular subtypes: characterization, validation, and prognostic value. PLoS Med 2013;10:e1001453.
28. Kim WJ, Kim EJ, Kim SK, Kim YJ, Ha YS, Jeong P, et al. Predictive value of progression-related gene classifier in primary non-muscle invasive bladder cancer. Mol. Cancer 2010;9:3.
29. Tothill RW, Tinker AV, George J, Brown R, Fox SB, Lade S, et al. Novel molecular subtypes of serous and endometrioid ovarian cancer linked to clinical outcome. Clin Cancer Res 2008;14:5198–208.
30. Curtis C, Shah SP, Chin SF, Turashvili G, Rueda OM, Dunning MJ, et al. The genomic and transcriptomic architecture of 2,000 breast tumours reveals novel subgroups. Nature 2012;486:346–52.
31. Hagemann T, Robinson SC, Schulz M, Trümper L, Balkwill FR, Binder C, et al. Enhanced invasiveness of breast cancer cell lines upon co-cultivation with macrophages is due to TNF-alpha dependent up-regulation of matrix metalloproteases. Carcinogenesis 2004;25:1543–9.
32. Papa S, Zazzeroni F, Fu YX, Bubici C, Alvarez K, Dean K, et al. Gadd45beta promotes hepatocyte survival during liver regeneration in mice by modulating JNK signaling. J Clin Invest 2008;118:1911–23.
33. Maeda S, Kamata H, Luo JL, Leffert H, Karin M. IKKβ couples hepatocyte death to cytokine-driven compensatory proliferation that promotes chemical hepatocarcinogenesis. Cell 2005;121:977–90.
34. Darani HY, Shirzad H, Mansoori F, Zabardast N, Mahmoodzadeh M. Effects of Toxoplasma gondii and Toxocara canis antigens on WEHI-164 fibrosarcoma growth in a mouse model. Korean J Parasitol 2009;47:175–7.
35. Van Rooijen N, Sanders A. Kupffer cell depletion by liposome-delivered drugs: comparative activity of intracellular clodronate, propamidine, and ethylenediaminetetraacetic acid. Hepatology 1996;23:1239–43.
36. Global Burden of Disease Cancer Collaboration. The Global Burden of Cancer 2013. JAMA Oncol 2015;1:505–27.
37. Dieu-Nosjean MC, Goc J, Giraldo NA, Sautès-Fridman C, Fridman WH. Tertiary lymphoid structures in cancer and beyond. Trends Immunol 2014;35:571–80.
38. Ley K, Pramod AB, Croft M, Ravichandran KS, Ting JP. How Mouse Macrophages Sense What Is Going On. Front Immunol 2016;7:204.
39. Sakurai T, Maeda S, Chang L, Karin M. Loss of hepatic NF-kappa B activity enhances chemical hepatocarcinogenesis through sustained c-Jun N-terminal kinase 1 activation. Proc Natl Acad Sci U S A 2006;103:10544–51.
40. He G, Yu GY, Temkin V, Ogata H, Kuntzen C, Sakurai T, et al. Hepatocyte IKKbeta/NF-kappaB inhibits tumor promotion and progression by preventing oxidative stress-driven STAT3 activation. Cancer Cell 2010;17:286–97.
41. Arthur JS, Ley SC. Mitogen-activated protein kinases in innate immunity. Nat Rev Immunol 2013;13:679–92.
42. Yang Y, Kim SC, Yu T, Yi YS, Rhee MH, Sung GH, et al. Functional roles of p38 mitogen-activated protein kinase in macrophage-mediated inflammatory responses. Mediators Inflamm 2014;2014:352371.
43. Gaillard SL, Secord AA, Monk B. The role of immune checkpoint inhibition in the treatment of ovarian cancer. Gynecol Oncol Res Pract 2016;3:11.
44. Harding JJ, Dika El, Abou-Alfa GK. Immunotherapy in hepatocellular carcinoma: Primed to make a difference? Cancer 2016;122:367–77.
45. Roberts SS, Chou AJ, Cheung NK. Immunotherapy of Childhood Sarcomas. Front Oncol 2016;5:181.
46. Fearon DT. Immune-suppressing cellular elements of the tumor microenvironment. Annu Rev Cancer Biol 2016;1:13.1–13.15.
47. Finkin S, Yuan D, Stein I, Taniguchi K, Weber A, Unger K, et al. Ectopic lymphoid structures function as microniches for tumor progenitor cells in hepatocellular carcinoma. Nat Immunol 2015;16:1235–44.
48. Schneider C, Teufel A, Yevsa T, Staib F, Hohmeyer A, Walenda G, et al. Adaptive immunity suppresses formation and progression of diethylnitrosamine-induced liver cancer. Gut 2012;61:1733–43.
49. Wada Y, Nakashima O, Kutami R, Yamamoto O, Kojiro M. Clinicopathological study on hepatocellular carcinoma with lymphocytic infiltration. Hepatology 1998;27:407–14.
50. Karin M.Whipping NF-κB to submission via GADD45 and MKK7. Cancer Cell 2014;26:447–49.

Published OnlineFirst December 26, 2017; DOI: 10.1158/0008-5472.CAN-17-1833

Cancer Research
The Journal of Cancer Research (1916–1930) | The American Journal of Cancer (1931–1940)

AACR American Association for Cancer Research

GADD45β Loss Ablates Innate Immunosuppression in Cancer

Daniela Verzella, Jason Bennett, Mariafausta Fischietti, et al.

Cancer Res 2018;78:1275-1292. Published OnlineFirst December 26, 2017.